Control of Single Axis Electromagnetic Levitation System

M.Sc. Thesis

in

Electrical-Electronics Engineering

University of Gaziantep

Supervisor
Assoc. Prof. Dr. Vedat Mehmet KARSLI

by

Ali Osman ARSLAN

August 2012

REPUBLIC OF TURKEY

UNIVERSITY OF GAZİANTEP
GRADUATE SCHOOL OF NATURAL & APPLIED SCIENCES
ELECTRICAL – ELECTRONICS ENGINEERING

Name of the thesis: Control of Single Axis Electromagnetic Levitation System
Name of the student: Ali Osman ARSLAN
Exam date: 24.08.2012
Approval of the Graduate School of Natural and Applied Sciences

Prof. Dr. Ramazan KOÇ

Director

I certify that this thesis satisfies all the requirements as a thesis for the degree of Master of Science.

Prof. Dr. Celal KORAŞLI

Head of Department

This is to certify that we have read this thesis and that in our consensus/majority opinion it is fully adequate, in scope and quality, as a thesis for the degree of Master of Science.

Assoc. Prof. Dr. Vedat Mehmet Karslı

Supervisor

Examining Committee Members

Prof. Dr. Ergun Erçelebi(Chairman) ....

Assoc. Prof. Dr. Vedat Mehmet Karslı ....

Asst. Prof. Dr. Kemal Delihacıoğlu ....

I hereby declare that all information in this document has been obtained and presented in accordance with academic rules and ethical conduct. I also declare that, as required by these rules and conduct, I have fully cited and referenced all material and results that are not original to this work.

Ali Osman ARSLAN

ABSTRACT

CONTROL OF SINGLE AXIS ELECTROMAGNETIC LEVITATION SYSTEM

ARSLAN, Ali Osman

M.Sc. in Electrical –Electronics Engineering

Supervisor: Assoc. Prof. Dr. Vedat Mehmet KARSLI

August 2012, 65 pages

One of the most attractive topics in engineering is Magnetic Levitation (Maglev). Maglev is an example of creating anti-gravity force. Maglev train is an application of this subject and single-axis electromagnetic suspension system (SAEMSS) is the first stage of them.

In this study, SAEMSS is studied in terms of mathematical modelling and controlling. Mathematical models of the SAEMSS with the solenoid-type and U-type electromagnets are derived. This model contains second order polynomial because of magnetic force equation. Therefore, system is nonlinear and cannot be controlled by using linear control techniques. To overcome this problem the nonlinear equation is linearized at the equilibrium distance using Taylor series expansion method. PD and phase-lead compensators are designed to control the linearized unstable system.

Hall-effect sensor is used in solenoid type electromagnetic levitation system (ELS) and inductive sensor used in U-type ELS. Microchips' dsPIC30F4011 is chosen to process the measurement data and to generate the control signals.

A metal ball or a permanent magnet disk is successfully levitated at the certain set position with desired performance criteria against gravity force. Results of the simulation and experimental works show that phase lead controller has better performance than PD controller for both systems.

Keywords: *magnetic levitation, Maglev, electromagnetic suspension, EMS, hall-effect sensor, inductive proximity sensor, dsPIC30F4011*

ÖZET

TEK EKSEN ELEKTROMANYETİK ASKI SİSTEMİNİN KONTROLÜ

ARSLAN, Ali Osman

Yüksek Lisans Tezi, Elektrik-Elektronik Mühendisliği Bölümü

Tez Yöneticisi: Doç. Dr. Vedat Mehmet KARSLI

Ağustos 2012, 65 sayfa

Manyetik olarak havaya kaldırma mühendislik alanında en çekici konulardan biridir. Yerçekimi kuvvetine karşı kuvvet üretmenin bir örneği manyetik askıdır. Manyetik olarak havada giden trenler bu konunun bir uygulamasıdır ve tek eksen manyetik askı sistemleri (TEMAS) bunun ilk aşamasıdır.

Bu çalışmada, matematiksel modelleme ve denetim açısından TEMAS çalışılmıştır. solenoid ve U-tip elektromıknatısları kullanılarak yapılan TEMAS' nin matematiksel modelleri türetilmiştir. Model manyetik alan kuvvetinden dolayı ikinci dereceden denklem içermektedir. Sistem doğrusal değildir ve doğrusal denetleme teknikleriyle denetlenemez. Bu sorunu aşmak için denklem Taylor seri açılımı metodu kullanılarak denge mesafesinde doğrusallaştırılır. Doğrusallaştırılmış kararsız sistemi denetlemek için oransal-türev ve faz ilerlemeli düzenleyiciler tasarlanır.

Hall-etkisi algılayıcı selonoid tip elektromanyetik askı sisteminde (MAS) kullanılırken endüktif algılayıcı U-tip MAS' da kullanıldı. Ölçüm verileri işleme ve kontrol sinyallerini üretmek için Microchip'in dsPIC30F4011'i kullanıldı.

Metal top veya sürekli mıknatıs disk yerçekimi kuvvetine karşı istenilen başarı ölçütleriyle denge konumunda başarılı bir şekilde askıda tutuldu. Deneysel ve benzetme çalışmalarının sonuçları faz-ilerlemeli denetleyicinin oransal-türev denetleyiciye nazaran bu istem için daha başarılı olduğu görüldü.

Anahtar Kelimeler: *manyetik askı sistemi, MAS, elektromanyetik askı sistemi, dsPIC30F4011, hall-etkisi algılayıcı, endüktif mesafe algılayıcı*

''To my wife and daughter''

ACKNOWLEDGEMENTS

First and most importantly I must thank the Most Merciful, Almighty ALLAH for making everything possible.

I would like to express my deepest gratitude to my supervisor Assoc. Prof. Dr. Vedat Mehmet KARSLI for his guidance, advice, criticism, encouragements and insight throughout this study.

Thanks also The Science and Technological Research Council of Türkiye (TUBITAK) to study the project 104M276.

Special thanks to my friends Mehmet DEMİR, Seydi KAÇMAZ, Berrin SÜSLÜOĞLU and Mehmet ARICI for their kind help, encouragement and patience during my study.

I would like to thank to my friends, Erhan ERSOY, Taner KARSLI, Mahmut AYKAÇ and Taner İNCE for supporting and encouraging me with their best wishes.

Thanks to technical staffs, and colleagues for their supports, especially Yusuf SEYFİ

I also wish to thank to my brother, İsmail Hakkı ARSLAN, and his wife, my sisters and her husbands and my wife's' family for believing in me.

Finally, I would like to express my love and appreciation to my wife, Leyla ARSLAN, my daughter, Meryem Sena ARSLAN, my parents, Ali ARSLAN and Yeter ARSLAN, who have created and maintained a wonderful life for me and contributed to my life with their lovely supports and encouragements.

TABLE OF CONTENTS

LIST OF FIGURES

LIST OF TABLES

LIST OF SYMBOLS/ABBREVIATIONS

MAGLEV: magnetic levitation

EMS: electromagnetic suspension

EDS: electrodynamic suspension

HEMS: hybrid electromagnetic suspension

SCM: superconducting magnet

PM: permanent magnet

dc: direct current

ADC: analog to digital conversion

MOSFET: metal-oxide-semiconductor field effect transistor

PC: personal computer

H^{∞}: Infinity hysteresis

PD: proportional derivative

PID: proportional integral derivative

MATLAB: matrix laboratory

GUI: graphical user interface

LED: light emitting diode

HIL: hardware in the loop

SISO: single input single output

NSGA: non-dominated sorting genetic algorithm

DSP: digital signal processor

MCU: microcontroller unit

PWM: pulse width modulated

IPS:	inductive proximity sensor
CNC:	computer numerical control
l:	mean length
A:	cross-sectional area
L:	inductance
R:	resistance
$\mathcal{R}$:	reluctance
MMF:	magneto motive force
N:	number of turn
ϕ:	magnetic flux
B:	magnetic field density
μ_0:	permeability of air
m:	mass
g:	acceleration of the gravity
a:	acceleration of an object
β:	sensor gain
V:	voltage
F:	force
i:	current
x:	distance
ξ:	damping ratio
w_n:	natural frequency
θ:	angle between two pole with respect to real axis of the complex plane
TF:	transfer function
K_c:	controller gain
K_p:	proportional gain
K_d:	derivative gain

K_i: integral gain

LCR: inductance capacitance resistance

RCD: resistor-capacitor-diode

RAM: random access memory

EEPROM: electrically erasable programmable read-only memory

MIPs: million instructions per second

PLL: phase locked loop

LCD: liquid crystal display

IDE: integrated development environment

CHAPTER 1

INTRODUCTION

Increasing of population and expansion in living zones combined with inadequate of existing transportation system expand the research of new-generation transportation systems. The innovative vehicle must meet certain requirements such as rapidity, reliability, and safety. In addition, it should be suitable, environment-friendly, low maintenance, compact, light-weight, unattained, and suited to load carrying. The magnetic levitation (MAGLEV) train is one of the best aspirants to assure those requisite. While a conventional train has serious friction problem between wheels and rails, the MAGLEV train didn't use wheels except start and stop of the travel and levitates on the guideway. It can work at very high and low speeds [1].

Nowadays super speed trains are designed to run on air suspension systems. By this way, the friction problem is minimized and the friction noise of classical railway trains is highly reduced. In order to solve both these problems there is a need to improve electromagnetically levitated systems.

For these reasons, this subject is selected to control a prototype of electromagnetic suspension (EMS) system which is supported by TUBITAK (The Science and Technological Research Council of Türkiye) with 104M276 project number.

The EMS system can be classified in three-types such as single-axis (like a point), half-bogie (like a line) and full-bogie types (like a plane). Levitation of ball with solenoid type coil is an example of single axis EMS and first stage for maglev train.

Single-axis EMS system is successfully operated and reported in the thesis. Second and final stages will be worked in future.

Electromagnetic suspension system is nonlinear inherently to overcome this problem; firstly system is linearized using, Taylor series expansion method. Mathematical model of single axis solenoid and u-type electromagnetic levitation system are derived with linear equation. PD and phase lead controllers are embedded to controller to control the levitated item at desired level.

Hall-effect and Inductive proximity sensors are used for detecting levitated object position. Microchips' dsPIC30F4011 is used as microcontroller that utilized 10-bit ADC to collect distance information and 16-bit PWM to control the switching devices and so electromagnet at desired position. Various circuits are utilized for building system and protecting components.

1.1 Overview of the Chapters

A brief review of the contents of this thesis is given as follows:

Chapter 2: It adverts about the Maglev and types and literature survey on electromagnetic suspension system.

Chapter 3: Mathematical models of the single-axis EMS system with solenoid-type and U-type electromagnets are derived using electrical, dynamics related to sensor, and magnetic relation. Transfer function is obtained.

Chapter 4: This chapter explains components that are used for composing EMS system.

Chapter 5: It mentions about the controller design using root locus technique. PD and phase lead compensator are designed to levitate the object at the equilibrium position and compared them.

Chapter 6: This chapter explains the used software programs that are utilized for microcontroller programming and for simulating the system.

Chapter 7: It mentions about the thesis conclusion and future plans.

.

CHAPTER 2

MAGLEV AND LITERATURE SURVEY

2.1 Introduction

Magnetic Levitation (MAGLEV) and types and literature review for EMS are mentioned in this chapter. Three types of the Maglev are discussed namely electromagnetic suspension, electrodynamic suspension and hybrid electromagnetic suspension. Electromagnetic suspension model is operated using magnetic attraction force between iron guideway and electromagnet. Electrodynamic suspension is applied utilizing repulsive force between two permanent magnets. Hybrid electromagnetic suspension model uses both magnetic forces. The details are given following sections.

2.2 Magnetic Levitation (Maglev)

The phenomenon of levitation has attracted attention from philosophers and scientists in the past. Magnetic levitation, maglev, or magnetic suspension is a method by which an object is suspended with no support other than magnetic fields.

There are three types of MAGLEV technologies namely:

-Electromagnetic suspension (EMS)

-Electrodynamic suspension (EDS)

-Hybrid electromagnetic suspension (HEMS).

2.2.1 Electromagnetic Suspension (EMS)

The levitation is performed using magnetic attraction force between electromagnet and iron guideway as shown in Figure 2.1. The system is nonlinear and open-loop unstable. The airgap of the controlled system is usually small like 10mm. If the speed increase, the control of the system becomes difficult. EMS is easier than EDS

technically. EMS system works with zero and high speed. In EMS, there are two types of technologies:

-Levitation and guidance integrated,-Levitation and guidance separated

The integrated one is suitable for low speed and low cost application because the number of electromagnet and controllers is reduced and guidance force is automatically produced by the difference of the reluctance. The integrated type of levitation consumes less electric power than the separated one.

In this type of the MAGLEV, for high speed interference between levitated train and guidance increases, so the control of the system will be difficult [1].

In separated levitation and guidance type, there is no interference between guidance and levitation. Therefore, it.is also preferred for high speed operation of the MAGLEV.

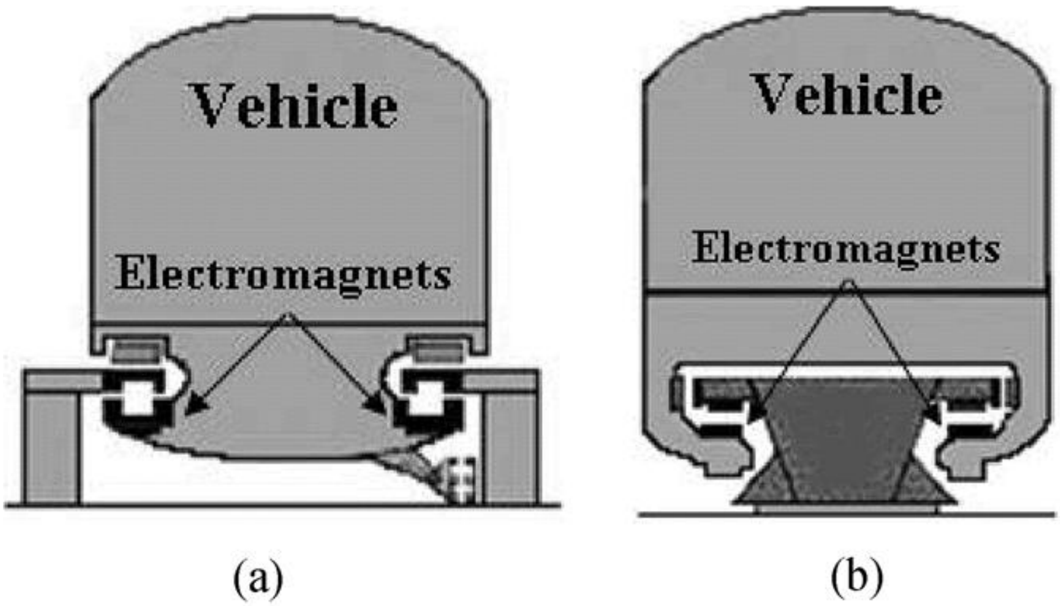

Figure 2. 1. Electromagnetic suspension **a)** levitation and guideway integrated **b)** levitation and guideway separated

2.2.2 Electrodynamic Suspension (EDS)

EDS uses repulsive force to levitation. The magnets placed on train carry forward on the inducing coils or conducting sheets that are located on the guideway, the induced currents flow through the coils or sheets and magnetic field is produced as shown in Figure 2.2. It is so stable magnetically and unnecessary to control airgap which is around 100mm. It is convenient for high speed operation and very secure for load variation. The enough speed (around 100km/h) is needed for adequate induced current for levitation. For low speed, train uses wheels such as starting and stops time. EDS can be divided in two types such as permanent magnet (PM) and superconducting magnet (SCM) types [1].

The structure of the PM is very simple. Electric power is not needed for this type. It is used for small system.

The structure of the SCM is very complex. Helium refrigerator is required for making the SCM operate. The SCM type holds a world speed record that is 581 km/h in 2003 in Japan [1].

2.2.3 Hybrid Electromagnetic Suspension (HEMS)

To reduce the power consumption of the EMS, permanent magnets are supported to electromagnet for levitation in this type PM is used for levitation of body and main load and electromagnet is used for airgap control. However the permeability of permanent magnet is equal to the air. So EMS needs much bigger amplitude of current than the HEMS.

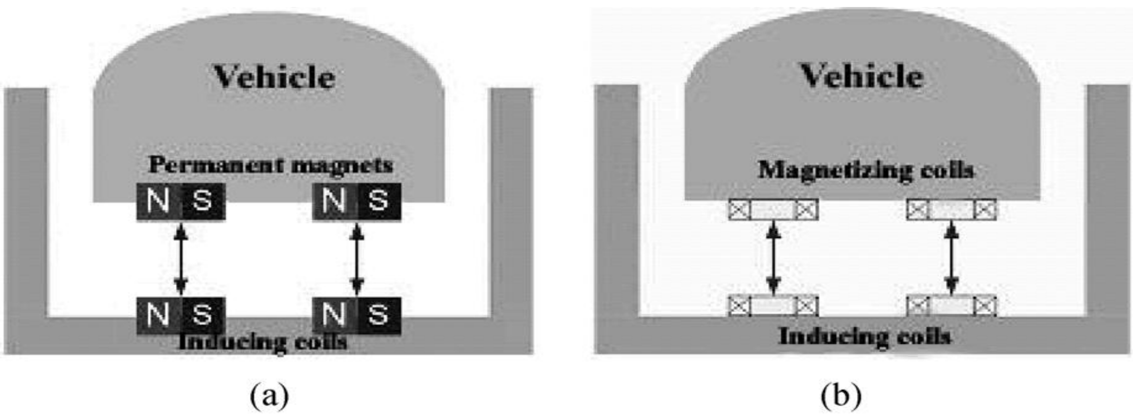

Figure 2. 2. Electrodynamic suspension **a)** using PM **b)** using SCM [1]

2.3 Literature Survey for EMS

The Maglev train can be reasonably dated from 1934 when Hermann Kemper of Germany patented it. After pass few decades, development of the Maglev train went through the acceleration time of the 1960s, the ripeness of the 1970s–1980s, and the trial period of the 1990s. Finally, MAGLEV train was completed as practical public service successfully in 2003 in Shanghai, China by Germany [1].

The first proposal for a dc controlled electromagnetic levitation by Graeminger (1912) with using U-shaped magnet core. A gap was to be measured between the electromagnet and the rail by a mechanical device which would alter a resistance in series with the magnet winding and this proposal didn't work in practical [2].

Anschutz- Kaempfe (1923b) then suggested contactless centering of a floated sphere containing gyro rotors using electromagnets. The resistance of the conductive fluid between the inner and outer spheres was measured to sense the distance between them. Alternating current was also used to supply to outer sphere so that the eddy currents induced in the inner sphere that was centered by repulsion [2].

Kemper (1934) proposed a system that was controlled current of the electromagnet. The proposed vehicle suspended by electromagnets attracting to the underside of a rail. The airgap was measured using capacitive or inductive means of sensing. Part of the circuit also yielded a voltage proportional to the rate of change of the airgap for damping of the vertical oscillations. This model is an interim scheme of the first and the present generation of suspension. Kemper constructed a system that consisting of an electromagnet with pole faces of 30 cm x 15 cm. The mass of the suspended model was 210 kg. The airgap and airgap flux density were 15mm and 0.25T, respectively. Power consumption of the system was 270W. This is the heaviest weight to be suspended using any method of electromagnetic suspension or levitation until the 1971 [2].

Much of the published work after that of Kemper on the development of the electromagnetic suspension scheme using controlled direct current (DC) electromagnets and external position sensing was at the University of Virginia, particularly on rotor suspensions. The other applications proposed were for testing bursting speeds of spheres such as ball bearings, testing adhesion of metal films, turbo-molecular pumps for use at high vacuum free of bearings requiring lubricants. The same principle has been used to suspend aircraft models in wind tunnels.

Wong T.H. (1986) built a magnetic levitation classroom demonstration device that was levitating a ball magnetically at the equilibrium position. Phase-lead compensation technique was used for control the unstable nonlinear system [3].

Morishita M, Azukizawa T, Kanda S, Tamura N and Yokoyama T(1989) developed a new electromagnetic suspension system that is energy saving. In this suspension system permanent magnet is used to levitate together with electromagnet. The electromagnet controlled the airgap and permanent magnet always balances the total weight of the vehicle and its load. The system is called hybrid model [4].

[Cho-Kato Spilman] (1993) in this paper single axis magnetic levitation system was investigated to compare sliding mode controller and integral plus phase-lead controller for stabilizing. In general, they said that the sliding mode controller was notable fine than the classical controller, even though additional system information about actuator dynamics was included to classical controller to improve the performance. They believed that the recent improvement on the robust and nonlinear control methods can be applied to assure better performance than the traditional methods [5].

Barie and Chaison(1996) made a study on the magnetic levitation with ball. In this study, a nonlinear controller based on exact feedback linearization theory was compared with a linear state-space controller in terms of tracking performance on the approximate linear model of the system. For step response, they used 8 and 12 bit analog to digital conversion (ADC). For 8 bit ADC, nonlinear controller is not good because of quantization error. However, when 12-bit ADC was used, simulation results showed that the performance of the nonlinear controller was equal to the linear controller. For sinusoidal reference signal, the nonlinear controller had better tracking performance than linear controller in terms of significantly smaller tracking error and ability to tracking higher-frequency trajectories [6].

Hurley and Wolfle (1997) designed a magnetic suspension system to provide a high impact visual demonstration of many principles those are electromagnetic design, compensation of open loop unstable system and power amplifier design in undergraduate educational programs in electrical engineering. The electromagnetic design included electromagnetic and dynamic analysis. Proportional plus derivative compensator was implemented using root locus and pole placement techniques. Metal-oxide-semiconductor field effect transistor (Mosfet) was used as power amplifier. All formulas had been derived from first principles [7].

Sahio (2001) reported on the design of controller for keeping a steel ball suspended in air. Transfer function of the system linearization and phase lead compensation were utilized to design the controller of the unstable nonlinear system. The offered algorithm was applied on robust closed-loop magnetic levitation system which can stabilize system with respect to different suspended mass variation. By ignoring higher order term of the magnetic force formula applying Taylor series expansion; the system becomes nearly linear and takes the floating airgap of the ball as a reference. The system was not good for great changing of the metal ball weight [8]

Hajjaji and Quladsine (2001) proposed a nonlinear model for magnetic levitation system which is validated with experimental measurements. Using this model, a nonlinear control law based on differential geometry is firstly synthesized. Then, its real-time implementation is developed. The control algorithm is implemented on a standard personal computer (PC)-type Pentium 90 MHz with an analog device PCL-812PG multifunctional board which has 12-bit resolution analog to digital conversion capable with 30 kHz sampling. The robustness test in terms of the variation of the mass was showed the good performance of the offered nonlinear control [9].

Shen (2002) studied H^{∞} control and sliding mode control of magnetic levitation system. A magnetic levitation kit was built and its model was feedback linearized. H^{∞}(Infinity hysteresis) control designed. Sliding mode controller and proportional-integral-derivative (PID) controller were designed for comparison. Setpoint regulation and tracking control experiments was performed on the designed controller. The performance of PID controller is quite good for reference signal tracking and disturbance suppressing. The performance of the H^{∞} control and sliding mode control were better than PID controller in trajectory tracking. The performance of the H^{∞} control was superior to sliding mode control. Feedback linearization method is good for designing nonlinear control system with large operational interval [10].

Yang, Miyazaki, Jin and Wada (2002) proposed an efficient physical parameter identification method for magnetic levitation system and robust nonlinear control via back stepping design approach for the system. Trajectory tracking performance was improved using new parameter identification method with respect to existing methods [11].

Gomes, Silva and Neto (2003) developed an electromagnetic suspension system at UFRJ using real time control toolbox available with matrix laboratory (MATLAB). This study indicated the model that was used in airgap control of a steel ball and the proportional-derivative (PD) control design procedure. For real time application PC and PCL-812PG Enhanced Multi-Lab Card were used. Position of the ball was detected using infra light-emitting-diode (LED) with phototransistor. The paper showed MATLAB's real time control toolbox is a powerful tool for control applications [12].

Shiakolas, Schenck, Piyabongkarn and Frangeskou(2004) implemented an interactive real-time digital controlled magnetic levitation system. MATLAB software package and its toolbox, a C++ Compiler and a nonlinear maglev system as hardware in the loop (HIL) device and graduate level nonlinear controls and neural network were implemented. Using this system, the students could easily compare the performance of the developed algorithms, discuss the merits of each algorithm, and decide which approach should be selected depending on the process requirements.

Sinha and Pechev (2004) study on the control of single axis electromagnetic suspension with using nonlinear H^{∞} state feedback and nonlinear H^{∞} output feedback controllers. Nonlinear H^{∞} control was applied firstly in this study. The difference between nonlinear state and the output feedback controllers is the execution time of the control algorithms 50 µs for the former and 400 µs for the latter (sampling interval of 1 ms).The survey of the performance of the new controller didn't complete yet [13].

Huajie and Jie (2004) devised a velocity filter to improve the stability of the electromagnetic suspension system. In this paper, the stability of the PD controller without filter was analyzed. The test oscillation condition was applied to the system in the simulation platform. The designed velocity filter influenced to reduce the noise and also improve the stability of the system [14].

Likemberg and Lundnerg (2004) built an electromagnetic levitation kit to teach control system design in an undergraduate course. The electromagnetic suspension device was marginally stable. Students were challenged to modify the system to develop the performance. The kit provided students with open-ended design problem [15].

Banerjee, Prasad and Pal (2006) designed and implement a single axis magnetic levitation system. The mass of the system is 14kg. The system is operated at desired point under ferromagnetic guideway. The vehicle has four electromagnetic actuators and four inductive proximity sensors each located at the corner of system. The actuators were controlled independently. MAGLEV was accomplished through the single input single output (SISO) control of each distance. Phase-lead controllers were used for current compensation at inner loop and overall system compensation at the outer loop for controlling of highly nonlinear and strongly unstable system. The prototype has been successfully designed and tested and stable levitation was showed experimentally at the reference airgap [16].

Yang and Pedersen (2006) implemented an automatic PID control design for single point magnetic levitation system. The controller is automatically tuned utilizing non-dominated sorting genetic algorithm (NSGA). The developed algorithm is applied in the TMS320C6713 Digital Signal Processor (DSP) digitally and was successful on the open-loop unstable and nonlinear system. The experimental result showed that the NSGA can be used for controlling complicated nonlinear system [17].

Gürleyen and Bahadır (2006) designed a PID controller that has two degree of freedom for electromagnetic levitation system. The controller was simulated in MATLAB platform and applied on the experimental setup. Using this controller system tracking performance and stability were shown to be good for levitation [18].

Öztürk, Kizir and Bingul (2007) designed and controlled single-axis EMS system. The nonlinear system was controlled using nonlinear feedback linearizing control technique and compared with linear control methods and was shown to be good that this method provides a wide variation of operation point against to linear one. For testing system performance, disturbances that have different frequencies were added vertically and horizontally to the system under different load condition. The controller rejected the both disturbances successfully [19].

Tang (2007) built one-dimensional and a two-dimensional electromagnetic levitation kits and applied real-time phase-lead control with analog and digital controllers. The electromagnetic force was accomplished by measuring the position of the object using hall-effect sensor and determined passing current in the electromagnet Analog controller was implemented using basic circuit elements with operational amplifier. Digital controller was achieved using TMS320CK6711 DSP. The system was controlled both analog and digital controller successfully on both one and two dimensional kits [20].

Guo, Li, Lu, Wang and Ye (2008) practiced a PID controller a single-axis ball HEMS. The system was hybrid because permanent magnet was used additionally for measuring ball position, supplied some of the needed electromagnetic force. A fixed-point DSP TMS320F2812 was chosen for its high speed and high efficiency of calculation and control. The DSP is widely used for power electronics and control applications. Both the simulation by MATLAB and real time control results showed the hybrid system worked well [21].

Deshpand and Mathur (2009) proposed a sensor that was used for detecting airgap distance. The most of paper reported that the implementation of optical sensor for detecting position of the object. These types of sensors needed to additional mountings that is difficult or may be sometimes impossible. The inductance is directly dependent on displacement. The developed sensor measured change in inductance of levitated electromagnet and indirectly measured distance. Using this sensor magnetic levitation system was implemented and operated on the reference airgap [22].

Wang, Jin and Liu (2009) performed sliding mode control method on feedback linearization suited to control one dimensional EMS system. The system with sliding mode control has rapid response, non-overshoot and strong interference suppression.

The output response of the controller was insensitive to parameter variations and external disturbances [23].

Ahmad and Javaid (2010) proposed a model for magnetic levitation system. Developed model was based on the inductance of the electromagnet coil. The inductance of the coil varied with inverse of the ball position. The simulation results for this model were good in the paper [24].

2.4 Summary

Magnetic Levitation is mainly applied two different principles by using magnetic attractive and magnetic repulsive force. If system is built using magnetic attractive force, system called as electromagnetic suspension system. Electrodynamics suspension system is named when repulsive force is used. If both principles are combined in a system, model can be termed as Hybrid.

EMS system applied on low and high speed and any long travel but EDS is proper for high speed and long travel. EMS is open loop unstable and nonlinear. However EDS is so stable magnetically. The control of the EMS is become difficulty with increasing speed. On the other hand, EMS is applied easier than EDS technically. Hybrid model contains advantages and disadvantages of both models. In terms of consuming energy for levitation, Hybrid model is efficient than EMS, but EDS is better than Hybrid model. Hybrid model is preferred in control perspective but in technically very difficult to implement Hybrid model.

EMS system is searched in all dimensions in the past papers. EMS is open loop unstable and nonlinear as mentioned above. Linearized model is used for controlling system at a desired position with linear control approach. PD, PID, phase-lead compensator are used to control the system. Nonlinear model is also utilized for same purpose using nonlinear control techniques. Both methods are successfully applied on the system. Hysteresis, on-off and sliding mode controller are also used for the system. System is operated with digital and analog controller.

CHAPTER 3

MATHEMATICAL REPRESENTATION OF THE SINGLE-AXIS ELECTROMAGNETIC LEVITATION SYSTEM

3.1 Introduction

In this chapter mathematical model of the single-axis electromagnetic levitation system is derived considering distance dependent dynamic, electrical and mechanical characteristics of the system. Electrical formula comes from Kirchhoff Voltage Law of the electrical circuit of the system. Dynamic formula is the net force on the system and can be represented by a distance dependent electromagnetic coil force and opposite gravitational force of the system. Distance information taken from a distance sensor is linearized for modeling linear function of the distance. Electromagnetic force formula represents that current passing though the coil produces electromagnetic forces. Current and Electromagnetic Force relation is second order polynomial. So the system is nonlinear. Firstly, system must be linearized to be able to control the system as desired using Linear Control Theory. Using Taylor Series Expansion technique, nonlinear relation of the system can be linearized with respect to the reference point. Obtained linear model of the system transforms into Laplace domain from time domain using Laplace transform. Then, Transfer Function (TF) can be obtained to divide output term to input term in Laplace domain.

A Transfer Function is the ratio of the output of a system to the input of a system, in the Laplace domain considering system's initial conditions and equilibrium point to be zero. The system must be linear and time-invariant to get transfer function. TF is a criterion to comment on stability, performance, response, and etc… characteristics of system.

3.2 Electrical Formula

The electrical circuit of the system shown in Figure 3.1 and relation between current and voltage of the circuit is derived using Kirchhoff Voltage Law. Coil can be expressed a series resistor and an inductor. Voltage drop on the resistor is $R.i(t)$ and inductor is $L\frac{di(t)}{dt}$. Applied voltage is equal to the summation of the voltage of the resistor and the inductor.

$$V_{app}(t) = R.i(t) + L\frac{di(t)}{dt} \tag{3.1}$$

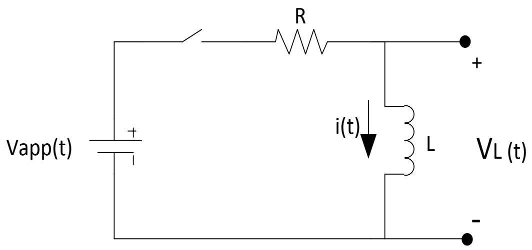

Figure 3. 1. Electrical circuit of the system

3.3 Electromagnetic Force Formula for U-type Electromagnet

We should determine electromagnetic force to levitate the system against the gravitational force. To obtain electromagnetic force that must be defined reluctance using cross-sectional area of core and air gap, magnetomotive force using current passing though the coil and number of turns, magnetic flux, magnetic flux density, respectively.

Used core is U-type. Reluctance of the core and air gap can be defined using mean length of the magnetic circuit, permeability of the core material, cross-sectional area of the core and air gap, and air gap length.

Mean length of the magnetic circuit obtained as following,

$$l_{core} = 0{,}72\ (m) \tag{3.2a}$$

$$l_{air} = x\ (m) \tag{3.2b}$$

$$l_{rail1} = 0{,}04\ (m) \tag{3.2c}$$

$$l_{rail2} = 0{,}16\ (m) \tag{3.2d}$$

and cross-sectional areas can be found as in equation (3.2).

$A_{core} = 0{,}0128$ (m^2) (3.3a)

$A_{air} = 0{,}0128$ (m^2) (3.3b)

$A_{rail1} = 0{,}0128$ (m^2) (3.3c)

$A_{rail2} = 0{,}0064$ (m^2) (3.3d)

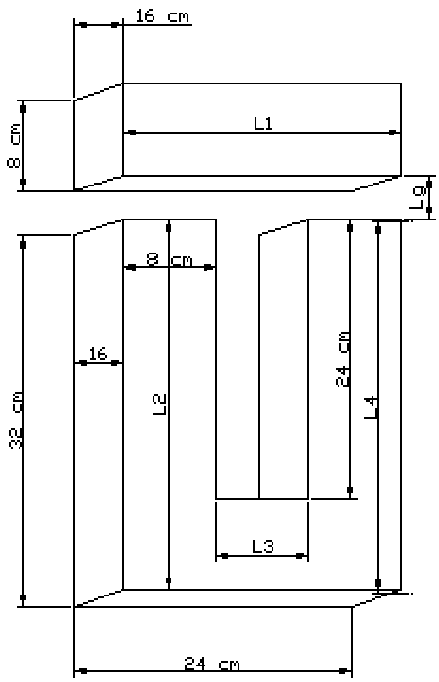

Figure 3. 2. Dimensions of the u-type core

Reluctance of the magnetic circuit can be written as:

$\mathcal{R}_{core} = \frac{l_{core}}{\mu_{r_{core}} \cdot \mu_0 \cdot A_{core}}$ (A.t/Wb) (3.4a)

$\mathcal{R}_{air} = \frac{l_{air}}{\mu_0 \cdot A_{air}}$ (A.t/Wb) (3.4b)

$\mathcal{R}_{rail1} = \frac{l_{rail1}}{\mu_{r_{rail}} \cdot \mu_0 \cdot A_{rail1}}$ (A.t/Wb) (3.4c)

$\mathcal{R}_{rail2} = \frac{l_{rail2}}{\mu_{r_{rail}} \cdot \mu_0 \cdot A_{rail2}}$ (A.t/Wb) (3.4d)

In magnetic circuit, all reluctances are in series, so total reluctance is denoted by the following equation.

$$\mathcal{R}_{total} = \mathcal{R}_{core} + \mathcal{R}_{rail1} + \mathcal{R}_{rail2} + 2\mathcal{R}_{air} \qquad (3.5)$$

Reluctance in air is dependent to air gap and other reluctance term is constant for core and rail, so total reluctance can be expressed as:

$$\mathcal{R}_{total} = K + 2\mathcal{R}_{air} \qquad (3.6)$$

Air reluctance term should be expanded and then total reluctance has the form as:

$$\mathcal{R}_{total} = K + \frac{2x}{\mu_0 . A_{air}} \qquad \text{(A.t/Wb)} \qquad (3.7)$$

Magnetomotive force is expressed in terms of coil turns and current passing through the coil is

$$MMF = N.i \qquad \text{(A.t)} \qquad (3.8)$$

Magnetic flux is the ratio of magnetomotive force to total reluctance as shown as:

$$\phi = \frac{MMF}{\mathcal{R}_{total}} \qquad \text{(Wb)} \qquad (3.9)$$

Magnetic flux term in (3.9) may be expanded using equation (3.8) and yields,

$$\phi = \frac{Ni}{K + \frac{2x}{\mu_0 A_{air}}} \qquad \text{(Wb)} \qquad (3.10)$$

In air, magnetic flux density is a ratio of magnetic flux to air cross-sectional area of the passing magnetic flux and denoted by

$$B = \frac{\phi}{A_{air}} \qquad \text{(Wb/m}^2\text{)} \qquad (3.11)$$

Magnetic flux density can be expanded using (3.10) and has the form as seen in (3.11)

$$B = \frac{\frac{Ni}{K + \frac{2x}{\mu_0 A_{air}}}}{A_{air}} \qquad \text{(Wb/m}^2\text{)} \qquad (3.12)$$

Electromagnetic Force is determined using $F_{mag} = \oint \vec{B}.\overrightarrow{dS}$ closed surface integral relation and is multiplied by two because electromagnetic force pulls the rail with two pole of the U-shaped core.

$$F_{mag} = 2\left(\frac{B^2 A_{air}}{2\mu_0}\right) \qquad \text{(N)} \qquad (3.13)$$

Magnetic force formula is rewritten using main terms of the system.

$$F_{mag} = \frac{\left(\frac{N.i}{KA_{air}+\frac{2x}{\mu_0}}\right)^2 A_{air}}{\mu_0} \qquad \text{(N)} \qquad (3.14)$$

Square term is expanded in the magnetic force equation as

$$F_{mag} = \frac{\mu_0 A_{air} N^2 i^2}{4x^2+4\mu_0 A_{air}+(\mu_0)^2(A_{air})^2K^2} \qquad \text{(N)} \qquad (3.15)$$

Magnetic force equation (3.15) can be written in terms of air gap distance between coil and rail, current passing though the coil, coil turns, cross sectional area of the magnetic flux in the air gap, air permeability, and constant reluctances. Constant terms in dividend of the equation (3.15) are very small with respect to $4x^2$ term, so we can neglect the constant term in the magnetic force formula.

$$F_{mag} = \frac{\mu_0 A_{air} N^2 i^2}{4x^2} \qquad \text{(N)} \qquad (3.16)$$

Magnetic force is rewritten in a simple form as:

$$F_{mag} = C\left(\frac{i}{x}\right)^2 \qquad \text{(N)} \qquad (3.17)$$

Constant term in the last form of the magnetic force equation can be expressed as:

$$C = \frac{\mu_0 A_{air} N^2}{4} \qquad (\text{Nm}^2/\text{A}^2) \qquad (3.18)$$

Finally the magnetic force is directly proportional with the square of current and inversely with the square of distance for U-type Electromagnet.

3.4 Electromagnetic Force Formula for Solenoid-Type Electromagnet

Electromagnetic force on the iron ball is determined by using following equation [13], [25], [26].

$$F_m = -\frac{I^2}{2} . \frac{dL}{dx} \qquad \text{(N)} \qquad (3.19)$$

where L is the inductance of the coil and x is the distance between ball and electromagnet.

Inductance of the electromagnet changes with respect to ball position. When ball is bring closer to electromagnet, total Inductance increases. If ball is far away the electromagnet, total inductance decreases. If ball is goes to infinity or there is no ball on the medium, minimum inductance can be measured. This inductance is self-inductance of the electromagnet. Total inductance under the effect of the ball is

$$L = L_1 + \frac{L_0 x_0}{x} \qquad \text{(H)} \qquad (3.20)$$

Where L_1 is the self-inductance of the electromagnet, L_0 is the mutual inductance with respect to ball at equilibrium position and x_0 is reference position [13].

Derivative of the total inductance is

$$\frac{dL}{dx} = \frac{d}{dx} . \left(L_1 + \frac{L_0 x_0}{x} \right) \qquad (3.21)$$

Yields,

$$\frac{dL}{dx} = -\frac{L_0 x_0}{x^2} \qquad (3.22)$$

Defined derivative of the total inductance in equation (3.19) is replaced by equation (3.20),

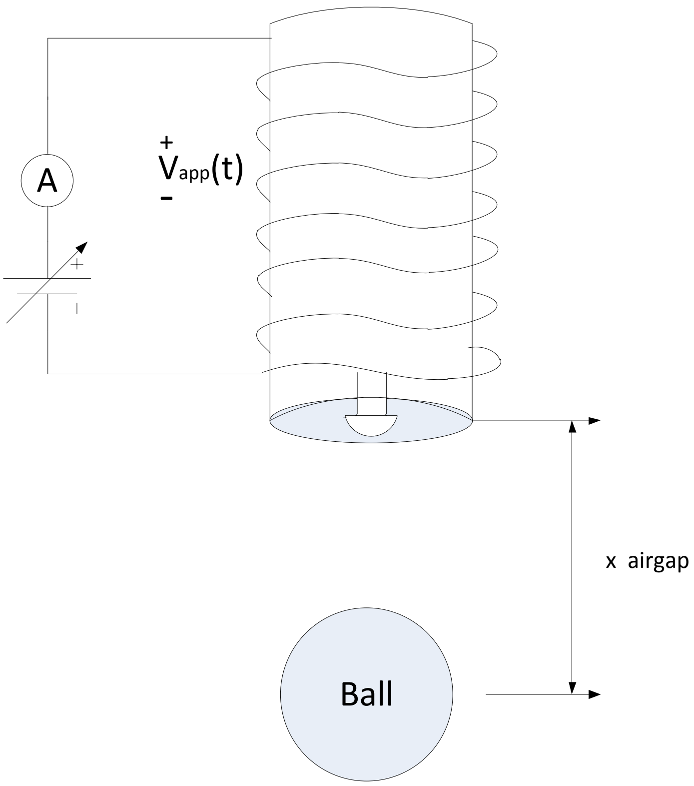

Figure 3. 3. A scheme of EMS using solenoid type electromagnet

$$F_m = -\frac{I^2}{2} . \left(\frac{L_0 x_0}{x^2}\right) \qquad \text{(N)} \qquad (3.23)$$

Rearrange the equation (3.23)

$$F_m = \frac{L_0 x_0}{2} . \left(\frac{I}{x}\right)^2 \qquad \text{(N)} \qquad (3.24)$$

Electromagnetic force formula is obtained. Electromagnetic force is proportional to square of current and inversely proportional to distance. Constant term is expressed as K, in equation (3.24). Magnetic force formula is rewritten as:

$$F_m = K . \left(\frac{I}{x}\right)^2 \qquad \text{(N)} \qquad (3.25)$$

Where $K = \frac{L_0 x_0}{2}$ that is the electromagnetic force constant for solenoid type electromagnet. The value of the K is found using equilibrium condition of the ball as equation (3.31)

Electromagnetic formula of the solenoid-type and U-type electromagnet has same formula and nonlinear characteristic because of square terms but constant term of them are different.

3.4 1 Linearization of Electromagnetic Force Formula

Magnetic force formula is second order polynomial, and not a linear equation. So the system is nonlinear. System cannot be stabilized using linear control techniques. Therefore, system must be linearized about a controllable reference point using Taylor Series Expansion [3], [8]. In the series expansion, higher order terms will be neglected to get linear equation.

General form of the Taylor Series Expansion is seen below;

$$f = f_0 + \frac{1}{1!}.\frac{df}{dx}.x + \frac{1}{2!}.\frac{d^2f}{dx^2}.x^2 + \frac{1}{3!}.\frac{d^3f}{dx^3}.+\ldots \qquad (3.26)$$

Constant and first order term is used for magnetic force formula in the control algorithm [3], [8], [19].

$$F_{mag} = F_0 + \frac{1}{1!}.\frac{dF}{d(x,i)}.(x,i) \qquad \text{(N)} \qquad (3.27)$$

Magnetic force is related to air gap distance and current. Last equation of the magnetic force is put into series and is differentiated by using partial differential operation with air gap distance and current:

$$F_{mag} = F_0 + \frac{1}{1!}.\frac{dF_{mag}}{di}.i + \frac{1}{1!}.\frac{dF_{mag}}{dx}.x \qquad \text{(N)} \qquad (3.28)$$

yields,

$$F_{mag} = C\left(\frac{i_0}{x_0}\right)^2 + \left[2C\frac{i_0}{(x_0)^2}\right]i - \left[2C\frac{(i_0)^2}{(x_0)^3}\right]x \qquad \text{(N)} \qquad (3.29)$$

Zero order (constant) term of the series can be used to determine the magnetic force at stable point.

$$F_0 = C\left(\frac{i_0}{x_0}\right)^2 \qquad \text{(N)} \qquad (3.30)$$

At reference point, magnetic force must be equal to the gravitational force on the system body under no-disturbance condition. The value of C can be found using following equation.

$$m.g = C\left(\frac{i_0}{x_0}\right)^2 \qquad \text{(N)} \qquad (3.31)$$

3.5 Dynamics Formula

Dynamics formula can be obtained using Newton's second law of motion of the system.

Net force (F_1) on the system is equal to gravitational force minus magnetic force,

$$F_{net} = F_{mg} - F_{mag} \qquad \text{(N)} \qquad (3.32)$$

and gravitational force is equal to the first order term of the magnetic force.

$$F_{net} = \left[2C\frac{(i_0)^2}{(x_0)^3}\right]x - \left[2C\frac{i_0}{(x_0)^2}\right]i \qquad \text{(N)} \qquad (3.33)$$

Net force in terms of distance and current is found. The net force is dependent to positive effect of distance and negative effect of current. If the system works at equilibrium position, net force on the system will be zero.

Net force is equal to the mass times acceleration of the system. Acceleration of the system is second derivative of the air gap distance as given as:

$$F_{net} = m.a \qquad \text{(N)} \qquad (3.34)$$

3.6 Sensor Formula

Feedback signal comes from distance sensor. To calibrate distance sensor, output voltage data is taken under different air gaps experimentally. Table 4.2 is filled using this output voltage and distance data. Output is normally estimated to a 3rd order polynomial function (see Figure 4.6). We must estimate a simple function to reduce the processing duration. So the linear region can be expressed in equation (3.35) by relation between output voltage of the distance sensor and air gap distance about the equilibrium position of the levitating object.

$$V_S = \beta . x \qquad \text{(V)} \qquad (3.35)$$

Where β is found as 234.4 using average slope of all output voltage of the distance sensor to air gap distance around the linear region of the distance curve. V_S is the distance information in volts and x is the distance in meters and the experimental data is given in Table 4.2.

3.7 Transfer Function

Transfer function of the system is a ratio of output to input in the Laplace domain. So, all equation of the system must be transformed into Laplace Domain using Laplace Transform.

Current and voltage relation is expressed as:

$$I(s) = \frac{V_{app}(s)}{R+sL} \qquad \text{(A)} \qquad (3.36)$$

Net force which is a function of distance and current derived in eqn. (3.33) can be expressed in Laplace domain as:

$$F_{net}(s) = \left[2C\frac{(i_0)^2}{(x_0)^3}\right]X(s) - \left[2C\frac{i_0}{(x_0)^2}\right]I(s) \qquad \text{(N)} \qquad (3.37)$$

Distance is related with mass and net force in Laplace:

$$X(s) = -\frac{F_{net}(s)}{ms^2} \qquad \text{(m)} \qquad (3.38)$$

Equation of the sensor 3.35 is in Laplace is expressed as:

$$V_S(s) = \beta X(s) \qquad \text{(V)} \qquad (3.39)$$

Finally, transfer function can be found using above equations. It is a ratio of sensor output voltage that is air gap distance information to input voltage is given using PWM technique.

$$G(s) = \frac{V_S(s)}{V_{app}(s)} \qquad (3.40)$$

And it is in terms of constants and parameters of the system.

$$G(s) = -\frac{\frac{2\beta C i_0}{mL(x_0)^2}}{\left(s+\frac{R}{L}\right)\left[s^2-\frac{2C(i_0)^2}{m(x_0)^3}\right]} \qquad (3.41)$$

Transfer function of the system is obtained numerically by replacing parameters with numerical values that is in Table 3.1.

$$G(s) = \frac{20406,66}{s^3+195,49\,s^2+1962\,s-383559,3} \qquad (3.42)$$

Obtained transfer function of the system has no zero and three poles. One of the poles is in unstable region of the complex plane. System is open-loop unstable.

Table 3. 1. Parameters of single axis magnetic levitation system for u-type electromagnet

<u>Parameters</u>	**<u>Values</u>**
Reference airgap (x_0)	0.01 m
Current at reference point (I_0)	11.87 A
Mass of the levitated system (m)	7.5 Kg
Force constant (C)	5.22e(-5) N.m^2/A^2
Resistance of the electromagnet (R)	3.87 Ohm
Inductance of the electromagnet (L_1)	19.79 mH
Sensor gain (β)	234.4V/m

Mathematical model of the system can be shown using state-space representation as:

$$\frac{dz}{dt} = \begin{bmatrix} -\frac{R}{L} & 0 & 0 \\ 0 & 0 & 1 \\ \frac{-2Ci_0}{m(x_0)^2} & \frac{2C(i_0)^2}{m(x_0)^3} & 0 \end{bmatrix} z + \begin{bmatrix} \frac{1}{L} \\ 0 \\ 0 \end{bmatrix} u \qquad (3.43)$$

$$y = [0 \quad \beta \quad 0].z \qquad (3.44)$$

State-space variable z represents a state vector $[i\ v\ x]^T$, where i is the current that passing through the coil, v is the velocity of the levitated object and x is the airgap distance.

3.8 Summary

Transfer function of the system is obtained by using Laplace domain relation of the electrical, dynamical, electromagnetic and sensor formulas. Normally, Electromagnetic force formula is second order polynomial, and cannot be controlled system using linear control theory. So this formula is linearized using Taylor series expansion method. Finally, all formula is transformed from time domain to Laplace domain using Laplace transform. Transfer function is the ratio of the proximity sensor output voltage to applied input voltage.

CHAPTER 4

EXPERIMENTAL SETUP AND COMPONENTS

4.1 Introduction

In this chapter, the experimental setup and its components are introduced in details. Figure 4.1 shows a schematic of the physical setup of the system.

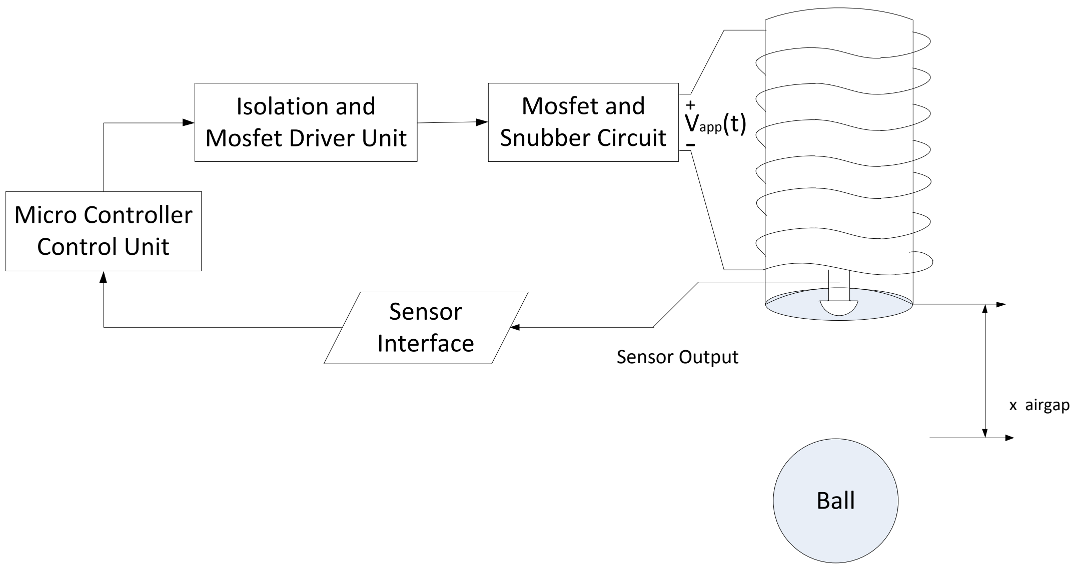

Figure 4. 1. Block diagram of physical system

The electromagnets, proximity sensors, Microcontroller, isolation and Mosfet circuit, power Mosfet and RCD snubber will be explained in the following sections.

4.2 Operation of the System

Electromagnet is used to produce anti-gravitational electromagnetic force. Proximity sensors measure the airgap distance and report the measured position data to the controller. ADC unit of the microcontroller (MCU) converts analog distance information to the digital one. MCU runs to apply control algorithm and to generate the output pulse width modulated (PWM) control signal to levitate the system at reference airgap. Isolation and Mosfet Driver Unit is made use of isolation between power voltage level and MCU voltage level and driving the Mosfet. Mosfet is a type of switching element for PWM signal. Snubber Circuit limits the overvoltage at breaking and overcurrent at conducting on the Mosfet and protects the switching element from harmful effects of electromagnetic inductor.

Used voltage levels are listed below. Isolated Power Supplies are used at different voltage levels.

Microcontroller	: 5 V dc
Optocoupler	: 5 V dc
Mosfet Driver	: 15 V dc
Electromagnet	: 24 V dc

4.3 Electromagnets

Electromagnet is a type of magnet. Current passing through the wire that is wrapped around the core produces magnetic field in the core. The direction of the magnetic field is found using right hand rule and is dependent to direction of the current. If you wrap fingers of your right hand around the coils in the direction of the current, your thumb indicates the direction of the magnetic field(from south pole to north pole of the electro magnet) When we change the polarity of the supply, the direction of the magnetic field will alter.

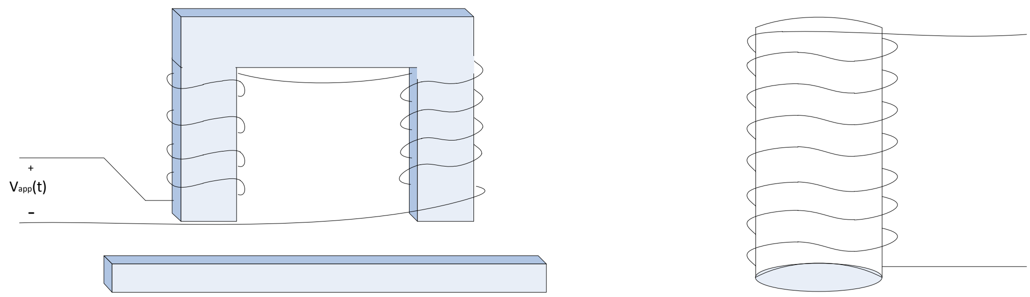

Figure 4. 2. Electromagnets

The coil's magnetic field is directly proportional to square of the number of turns and the coil current (see equation 3.16). It is easy to maximize keep piling on turns, and increasing the current.

For U-type electromagnet dimensions of the electromagnets are given in Figure 3.2, number of the turns is 280t. Values of inductance and resistance of the coil are 19.79 mH and 3.87 Ω, respectively.

For solenoid type electromagnet, number of turns is 1100t. Inductance and resistance of the electromagnet are 38.81mH, and 2.4 Ω. These values are measured using LCR meters.

4.4 Proximity Sensors

There are many types of the proximity sensors to get airgap distance. For this system, inductive, laser, resistive, IR and hall-effect sensors can be used. For the system hall-effect and inductive sensors are used to get distance information.

4.4.1 Hall-Effect Sensor

Dr. Edwin Hall searched out the hall-effect in 1879 but has only been put to noticeable use in the last three decades [27]. Today, Hall-effect devices are included in many products, ranging from computers to sewing machines, automobiles to aircraft, and machine tools to medical equipment. The Hall element is constructed from a thin sheet of conductive material with output connections perpendicular to the direction of current flow. When subjected to a magnetic field, it responds with an output voltage proportional to the magnetic field strength. The voltage output is very small (µV) and requires additional electronics to achieve useful voltage levels. When the Hall element is combined with the associated electronics, it forms a Hall-effect sensor [27].

Allegro UGN3503 (see Figure 4.3a) [28] Hall-effect sensors accurately track extremely small changes in magnetic flux density changes generally too small to operate Hall-effect switches.

Each Hall-effect integrated circuit includes a Hall sensing element, linear amplifier, and emitter-follower output stage (shown in Figure 4.3b). Hall-effect sensor operates two different modes with respect to reference magnetic pole. At rest (B=0) output voltage is half of supply voltage. If sensor operates with south magnetic pole, the output voltage is greater than the rest condition. Otherwise output voltage of the sensor is less than the resting condition. The sensor is placed bottom side of the electromagnet. In Table 4.1 the electrical characteristics of the sensor is shown. The sensor also has a flat response to 23 kHz. The Sensor is operated for 0-2.5V output voltage range.

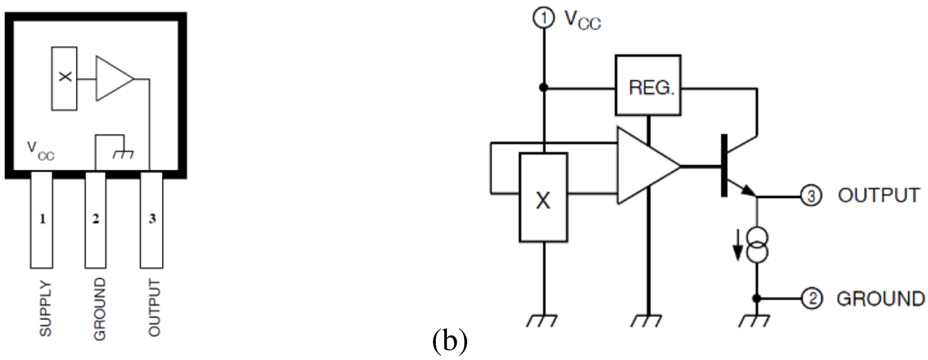

Figure 4. 3. a) Allegro UGN3503 radiometric linear Hall-effect sensor

b) Functional block diagram of UGN3503

Table 4. 1.Electrical characteristics of UGN3503 at T= 25°C

Characteristic	Symbol	Test Conditions	Limits Min.	Limits Typ.	Limits Max.	Units
Operating Voltage	V_{CC}		4.5	—	6.0	V
Supply Current	I_{CC}		—	9.0	13	mA
Quiescent Output Voltage	V_{OUT}	B = 0 G	2.25	2.50	2.75	V
Sensitivity	ΔV_{OUT}	B = 0 G to ±900 G	0.75	1.30	1.75	mV/G
Bandwidth (-3 dB)	BW		—	23	—	kHz
Broadband Output Noise	V_{out}	BW = 10 Hz to 10 kHz	—	90	—	µV
Output Resistance	R_{OUT}		—	50	220	Ω

4.4.2 Inductive Proximity Sensor (IPS)

An inductive proximity sensor (see Figure 4.4) consists of ferrite core with coils, oscillator, detector and output filter. The Oscillator generates high frequency alternating signal for coils on the ferrite core and magnetic field is produced around the coil. This field is emitted at the sensing face of the sensor. If a metallic or magnetic object nears the sensing face, eddy currents are generated. Target object interrupt the eddy current and reduce the output voltage of the oscillator circuit. The detector detects the oscillator output voltage and compares the reference voltage.

Last circuit of the sensor generates an output signal that gives distance information [29].

IPSs are solid-state devices that generate output signal with respect to metal object's distance. Physical contact is not required. IPS has best work with ferrous metals but they also work well with non- ferrous metals at small distance [29].

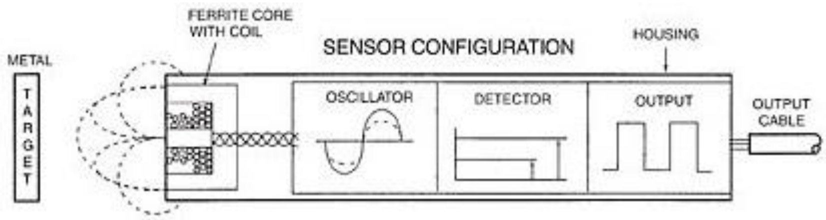

Figure 4. 4. Internal block diagram of the IPS

Their application ranges from Automobile Industries to Steel Industries, from Computer Numerical Control (CNC) machines to material handling equipment, process automation, conveyor systems and packaging machines.

For the system Telemecanique XS4-P30AB110 Inductive Proximity Sensor [30] is used to detect air gap. This sensor has 3-cable connection (Supply, Ground and Output). Sensor supply voltage is 15-30 Volt DC. The sensor runs with 15 V DC. At the output of the sensor is connected to 1kΩ resistor. The voltage on the resistor is measured for distance information. Experimentally, the output voltage on the resistor is collected with changing target's distance from face of the sensor (see Table 4.2).

Figure 4. 5. Telemecanique XS4-P30AB110 Inductive Proximity Sensor

Using MATLAB curve fitting tool-box output voltage- distance curve is obtained. This curve is fitted a 3rd order polynomial is given eqn. (4.1) and shown in Figure 4.6.

$$y = (-1E + 06)x^3 + 38925x^2 - 16,216x - 0,0229 \quad (4.1)$$

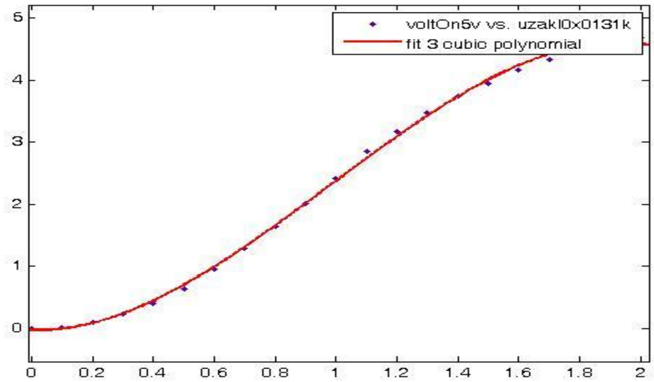

Figure 4. 6. Output voltage of the sensor with distance

This polynomial is not used to speed up the processing time of MCU. Relation between output voltage of the sensor and distance is supposed as a linear equation. The average slope of the curve is the gain of the sensor. Sensor gain can be determined using differentiation at all sensing region. The gain of the sensor is found as β=234.4.Sensor output voltage is beta multiplied by airgap distance.

Table 4. 2. Inductive proximity sensor voltage-distance data

Distance (x) (mm)	Voltage (Vs) (volt)	Slope (β) (V/m)
20	4,69	70
19	4,62	150
18	4,47	140
17	4,33	160
16	4,17	230
15	3,94	190
14	3,75	270
13	3,48	310
12	3,17	320
11	2,85	430
010	2,42	410
9	2,01	360
8	1,65	350
7	1,3	350
6	0,95	310
5	0,64	230
4	0,41	170
3	0,24	140
2	0,1	82
1	0,018	16
0	0,002	
	Gain (Average Slope) →	**234,4**

4.5 Microcontroller

Microchip dsPIC30F4011 is used as a microcontroller [31]. dsPIC is used for analog to digital conversion of distance information, processing control algorithm and generating control PWM signal. Analog distance information that is coming from proximity sensor is converted to 10-bit digital information. It compares instantaneous distance with reference distance and determines error info. PID algorithm is applied and 16-bit, 4 kHz PWM control signal is produced by duty cycle generators of dsPIC. Control parameters and duty are sent to the 4*20 LCD and can be read on the screen of the LCD. The pin configuration of the dsPIC30F4011 is given in Figure 4.7 and the appearance of the MCU circuit is shown in Figure 4.8.

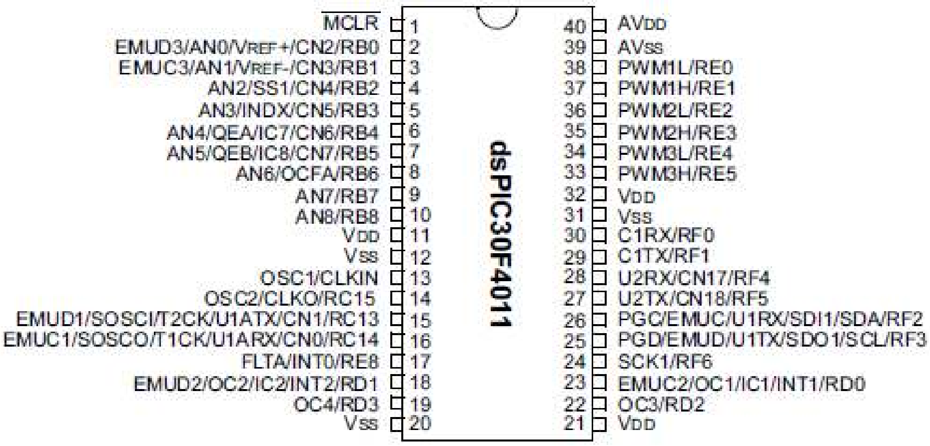

Figure 4. 7. dsPIC30F4011 pin diagram

Some features of the dsPIC are listed below.

• 48 Kbytes on-chip Flash program space

• 2 Kbytes of on-chip data RAM

• 1 Kbytes of non-volatile data EEPROM

• Up to 30 MIPs with PLL active (4x, 8x, 16x), max 120MHz

•Supply voltage: 5V

• High current sink/source I/O pins: 25 mA/25 mA

•Five 16-bit timers/counters; optionally pair 16-bit timers into 32-bit timer modules

• 16-bit Compare/PWM output functions

• 6 PWM output channels

• 3 duty cycle generators

• 10-bit Analog-to-Digital Converter (A/D) with 500 Ksps conversion rate

Figure 4. 8. A photo of MCU circuit with LCD

4.6 Isolation and MOSFET Driver Circuit

Isolation and MOSFET driver circuit is composed mainly two-part. Isolation part is used to isolate two different voltage levels. Optocoupler (Toshiba 6N137) is used for isolation. 6N137 includes a high emitting photo diode and a receiver circuits. Output of the 6N137 has a nand-gate. So the output signal of the 6N137 is inverted (see Figure 4.9) [32].

The speed of the 6n137 is very high. Operating temperature is between 0 °C and 70 °C. 6N137 has a high isolation voltage up to 2500 Vrms

BC237 npn transistor [33] is used to invert the output signal of the optocoupler and to supply enough current to drive the Mosfet Driver (MIC4422).

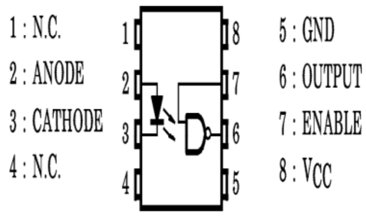

Figure 4. 9. Internal schematics and pin configuration of the 6N137

Second part of the circuit is Mosfet driver. MICREL MIC4422 is a non-inverting Mosfet driver. Pin Configuration diagram is given in Figure 4.10.The MIC4422 accepts any logic input from 2.4V to VS without external speed-up capacitors or resistor networks. It has matched rise and fall times (25ns), input will withstand negative swing of up to 5V, wide operating range 4.5V to 18V, high capacitive load drive 47,000pF, low delay time 30ns typically, high peak output current 9A peak and can drive the largest MOSFETs with an improved safe operating margin [34].

Proprietary circuits allow the input to swing negative by as much as 5V without damaging the part. Additional circuits protect against damage from electrostatic discharge.

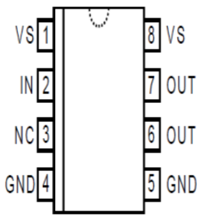

Figure 4. 10. Pin configuration of the MIC4422

MIC4422 can be used for Switch Mode Power Supplies, Motor Controls, Pulse Transformer Driver, Class-D Switching Amplifiers, Line Drivers, Driving MOSFET or IGBT Parallel Chip Modules, Local Power ON/OFF Switch and Pulse Generators applications. Isolation and Mosfet Driver Circuit and its PCB circuit are given in Figures 4.11 and 4.12. A photo of the actual circuit is placed in Figure 4.13.

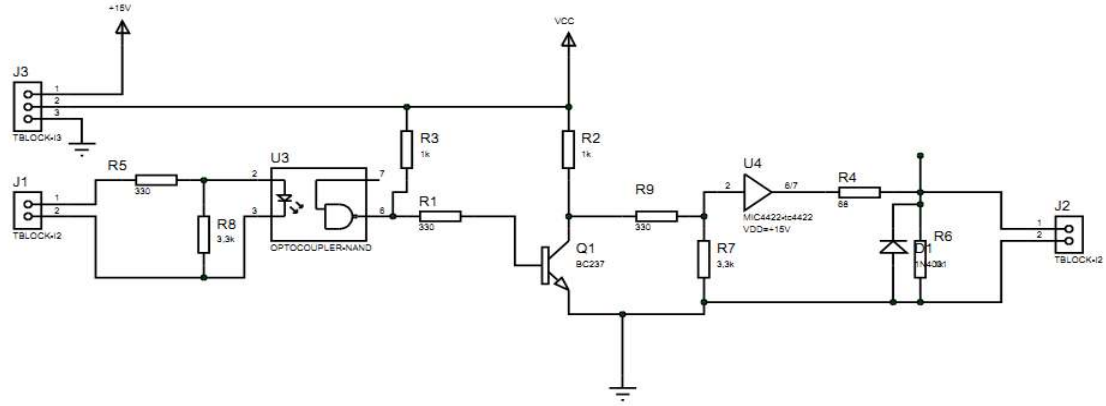

Figure 4. 11. Isolation and Mosfet driver circuit

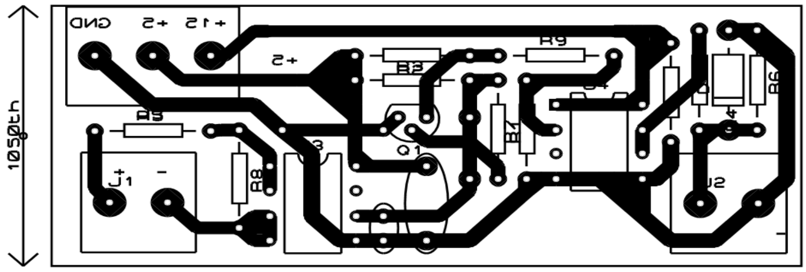

Figure 4. 12. Layout of isolation and Mosfet driver circuit

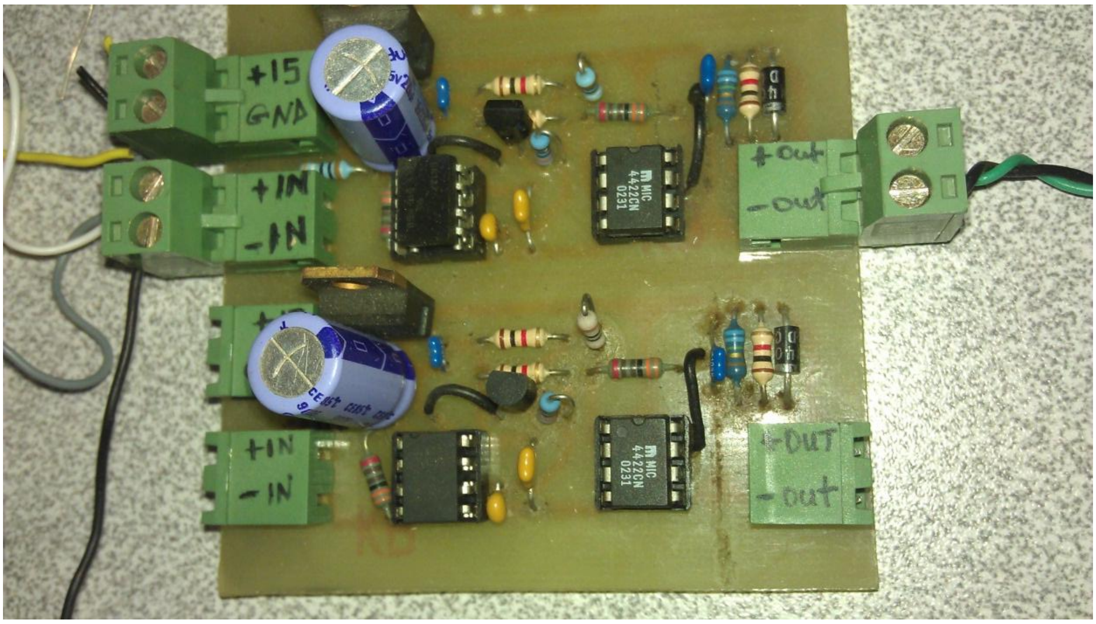

Figure 4. 13. An apperance of isolation and Mosfet driver circuit

4.7 Power MOSFET

The power metal oxide semiconductor field-effect transistor (Mosfet) is a switching device derived from the field-effect transistor for use as a fast-acting switch at power levels. Unlike bipolar transistor is current controlled, the Mosfet is a voltage-controlled device. The main terminals are the drain and source the current flow from drain to source being controlled by the gate to source voltage. The gate voltage determines the depth of the induced channel and in this manner determines the current flow. [35]

IXYS IXTQ170N10P Power Mosfet is used as a switching device in the system. The Mosfet has smaller than 9mΩ drain to source resistance, low package inductance, 100 V maximum supply voltage and 170A maximum drain-current. The gate voltage is between 15V and 30V [36].

The Mosfet can be used for switch-mode and resonant-mode power supplies, dc-dc converters, laser drivers, ac and dc motor drives and robotics and servo controls applications.

4.8 RCD Snubber

Snubbers are circuits which are placed across and in series with the switching device for protection and to improve performance. Snubbers can reduce or eliminate voltage or current spikes, limit di/dt or dv/dt, shape the load line to keep it within the safe operating area, transfer power dissipation from the switch to a resistor or a useful load, reduce total losses due to switching and reduce electromagnetic interface by damping voltage and current ringing [37].

There are many kinds of Snubbers. Resistor-capacitor-diode (RCD) turn-off Snubber is used in the system (see Figure 4.14 for circuit and Figure 4.15 for soldered snubber circuit).

When switch is turn-off, Snubber diode (Ds) shorts out the snubber resistance (Rs) and some of the supply voltage across the Snubber capacitance (Cs). Switching device is saved from over voltage.

When switch is turn-on, the voltage on the Cs is discharged across the Rs.

Cs is determined using equation (4.2),

$$C_s = \frac{I_0 t_s}{2E_0}\,\mathrm{F} \qquad (4.2)$$

where I_0 is reference current, ts is the fall time of the switch and E_0 is supply voltage of the Electromagnet.

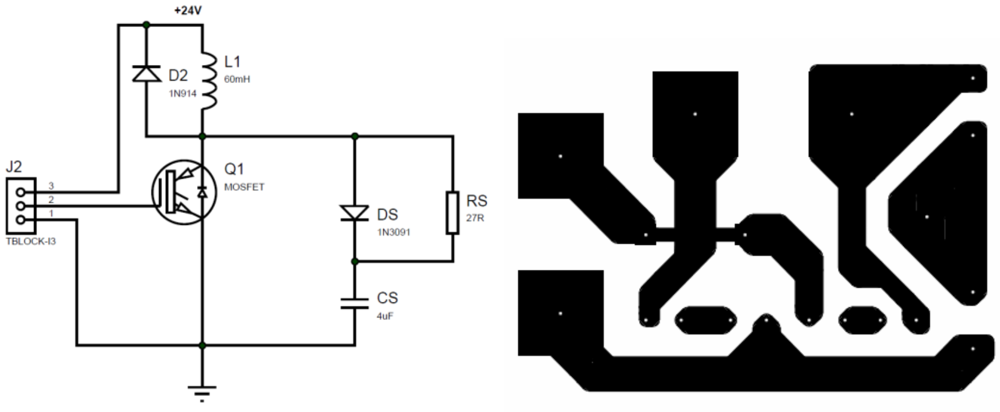

Figure 4. 14. The circuit and the layout schematic for RCD snubber

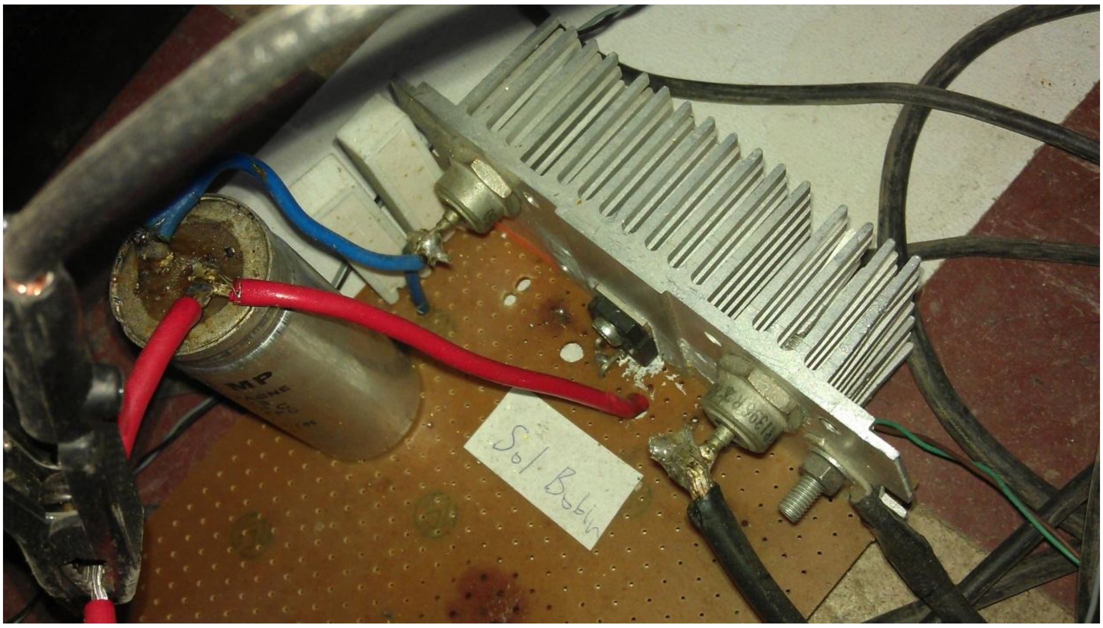

Figure 4. 15. Snubber circuit with Power Mosfet

Reference current is 12A, fall time is 10^{-5}s and suppy voltage is 24 V. Capacitance of the snubber is found as 2.5μF.

Snubber resistance is determined using following equation,

$$R_s = \frac{t_{on\,min}}{5C_s}\,\Omega \quad (4.3)$$

where minimum turn-on time of the switching device ($t_{on\ min}$) is about 10/1024 of the 4 kHz PWM . R_S is found as 20Ω.

4.9 Summary

In this chapter, the experimental setup and its components explain. The working schematic of the system is given in Figure 4.1. Electromagnet is introduced and its electrical values are measured using LCR meter. Used Proximity sensors are introduced in detail, gain of the sensor is obtained. dsPIC30F4011 is used to get analog distance information from proximity sensor and convert 10-bit digital one. It determines some control parameters and generate PWM control signal. Generated control signal is sent to switching device (Power MOSFET) across isolation and driver circuit. Isolation section of this card separates microcontroller and power voltage levels using optocoupler. Driver section of the card is used to produce enough current to drive the Power MOSFET. The switching device controls the current that is passing across the electromagnet. Snubber circuit protects the Power MOSFET from overvoltage and overcurrent and has many useful effects on the system. Its parameters are computed

CHAPTER 5

CONTROLLER DESIGN

5.1 Introduction

In this chapter, root locus graph is plotted using transfer function of the single axis magnetic levitation system. A pole of the plant is right-half plane of the root locus. So the system is unstable and a controller must be designed to transfer the pole to stable region. PD and phase-lead controllers are designed to stable the system and to satisfy the performance criteria. Performances of the designed controllers are compared with each other. The controller scheme is shown in Figure 5.1.

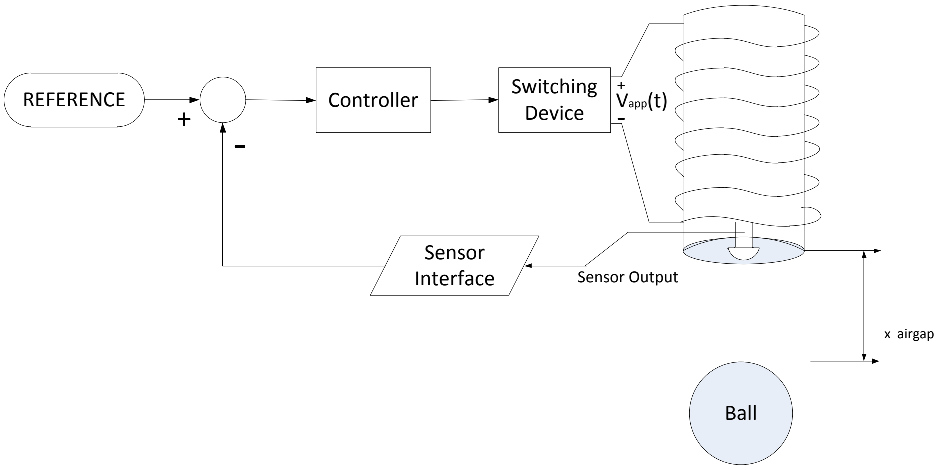

Figure 5. 1. Control scheme of the single-axis magnetic levitation system

5.2 Root-Locus Approach to Control System Design

The root-locus method is a graphical method for determining the locations of all closed loop poles from knowledge of the locations of the open-loop poles and zeros as some parameters are varied from zero to infinity. The method yields a clear indication of the effects of parameter adjustment. An advantage of the root-locus method is that it can be possible to obtain information on the transient response as well as on the frequency response from the pole-zero configuration of the system in the *s* domain. In practice, the root-locus plot of a system may indicate that the desired performance cannot be achieved just by adjustment of gain.

In fact, in some cases, the system may not be stable for all values of gain. Then it is necessary to reshape the root loci to meet the performance specification [38].

In designing a control system, if other than a gain adjustment is required; the original root loci must be modified by inserting a suitable compensator. Once the effects on the root locus of addition of poles and/or zeros are fully understood, the location of the poles and zeros of the compensator can be determined and the root locus will be reshaped as desired. In essence, in the design via the root loci of the system are reshaped through the use of a compensator so that a pair of dominant closed-loop poles can be placed at the desired location. Often, the damping ratio and undamped natural frequency of a pair of dominant closed-loop poles are specified [38].

The addition of a pole to the open-loop transfer function has an effect of pulling the root locus to the right, tending to lower the system's relative stability and to slow down the settling of the response.

The addition of a zero to the open-loop transfer function has an effect of pulling the root locus to the left, tending to make the system more stable and to speed up the settling of the response.

5.3 Uncontrolled System

System transfer function is given in equation (3.35), numerator of the transfer function is constant and its denominator is third order polynomial. So transfer function has no zero and three-pole.

$$G(s) = \frac{63262{,}6064}{s^3 + 195{,}5\, s^2 + 1995{,}85\, s - 390176{,}77} \qquad (3.35)$$

These poles of the system are

$S_1 = -195.494$ $S_2 = -44.2945$ $S_3 = 44.2945$

and S_3 is right-half plane of the root loci of the system as seen in Figure 5.2 using *rlocus* command in MATLAB [39].

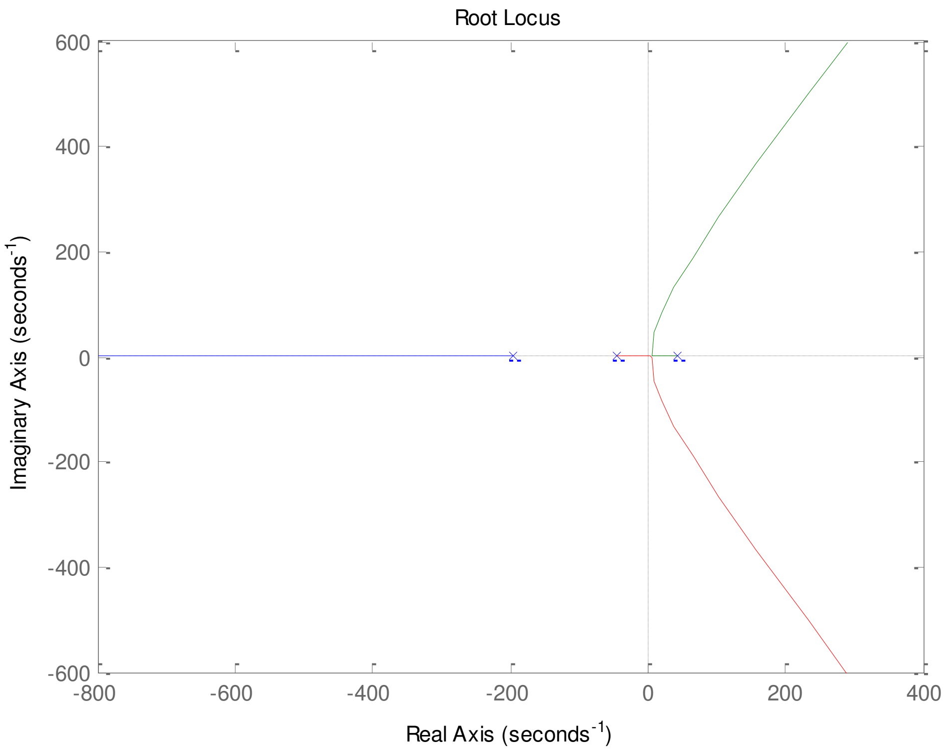

Figure 5. 2. Root locus of the system

The pole must be cancelled or transferred to left-half plane (stable region). Uncontrolled system step response is drawn using *step* command as seen in Figure 5.3. Step response curve goes to infinity without controller or with only proportional controller. It shows the system is unstable. The object cannot be set to desired reference point.

Impulse response of the uncontrolled system is given in Figure 5.4 using *impulse* command. Impulse response represents the reaction of the system at presence of any disturbance. Uncontrolled system impulse function goes to infinity with respect to disturbance. System is uncontrolled without controller. Controller must be designed to stable the plant with desired performance criteria.

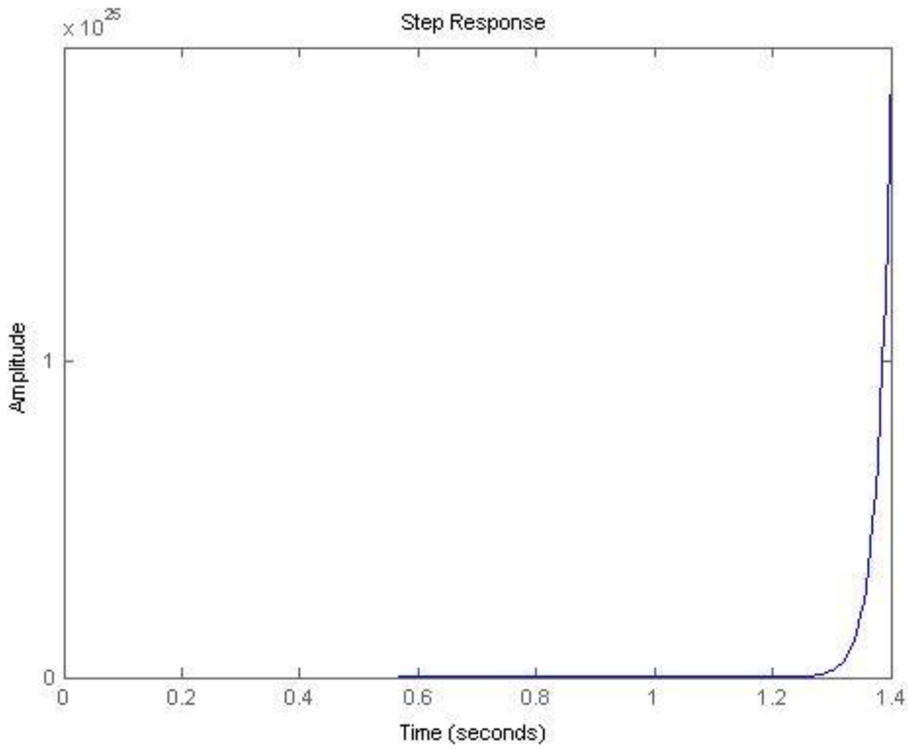

Figure 5. 3. Step response of the uncontrolled system TF

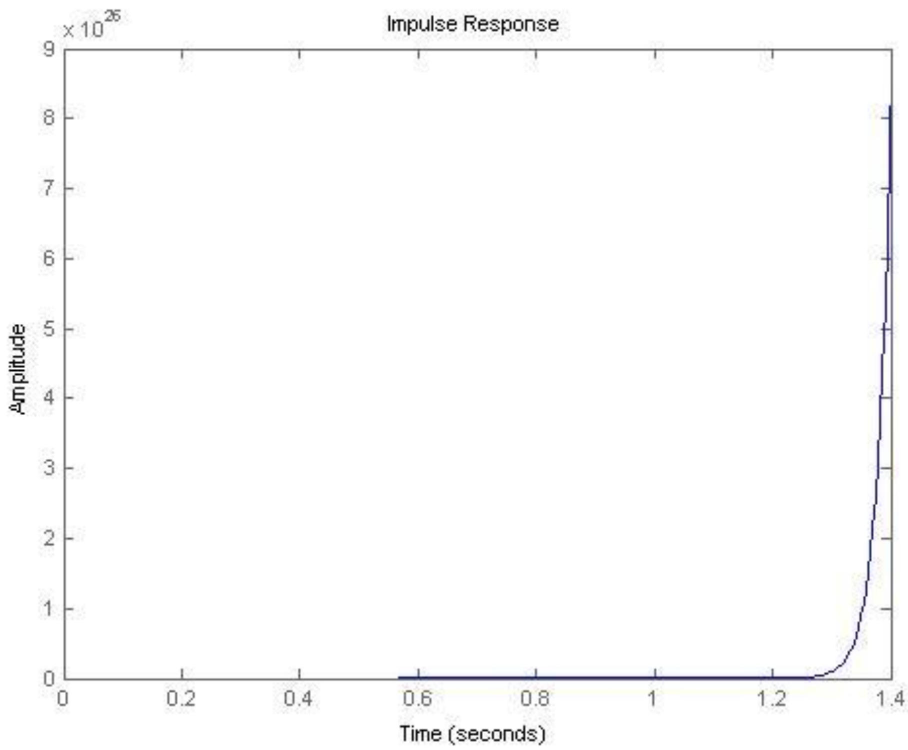

Figure 5. 4. Impulse response of the uncontrolled system TF

5.4 Performance Criteria

The requirements imposed on the control system are usually spelled out as performance criteria. Natural frequency and damping ratio are the performance criteria for a system [38]. Performance parameters (damping ratio and natural frequency) must be defined for wanted performance. Damping ratio ξ is selected as 0.7 (a value between 0.4 and 0.8 is preferred) [38]. For constant value of the naturel frequency, step response for second order system can be seen in Figure 5.5 with respect to damping ratio.

Natural frequency (w_n) of the system is 25rad.s^{-1}. Dominant poles in the complex plane are

$$s_{d_{1,2}} = -\xi w_n \pm j w_n \sqrt{1-\xi^2} \qquad (5.1)$$

and they are determined using intended performance criteria. Using the numerical values (w_n = 25rad/sec and ξ = 0.7) of the closed-loop dominant poles at

$$s_{d_{1,2}} = -17.5 \pm j\,17.85 \qquad (5.2)$$

are placed to the s-plane. The designer must use the dominant poles to compensate system for desired performance criteria.

5.5 Controller Design

Control systems are designed to perform specific tasks. Designed system should exhibit as small errors as possible in responding to the input signal. The damping of the system should be reasonable. The undesirable disturbance should be well attenuated.

For this system PD or phase-lead controller must be design as explained in following sections.

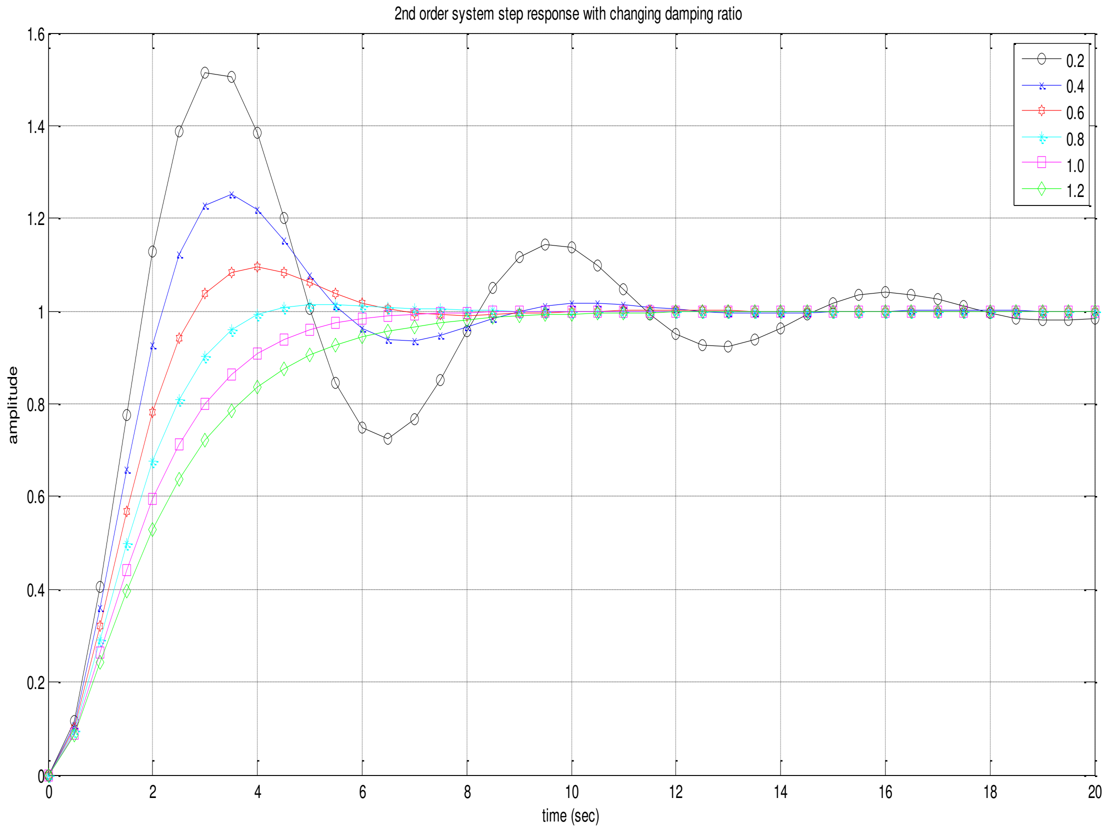

Figure 5. 5. Step response with respect to damping ratio

5.5.1 PD Controller Design

PD controller adds a zero to the system, the root loci of the system is pulling to the left. System is made stable. Settling time of the system is decreased. Right half-plane pole is cancelled.

PD controller is

$$G_c(s) = K_c(s + z) \tag{5.3}$$

where K_c is the gain of the controller and z is the zero of the controller in s domain.

Dominant poles are determined using desired performance specification and located on the complex plane.

PD controller adds only zero on the σ-axis. The location of the zero can be found using total angles of the poles and zeros with respect to any zero or pole. Total angles are equal to the 180k, where k is an integer (see Figure 5.6) [38].

Controller angle is determines using angle of other poles of the system. The angle of zero is positive and angles of poles are negative. Addition of the angles is equal to the -180 degree.

$$\theta_c - \theta_{p1} - \theta_{p2} - \theta_{p3} = -180° \tag{5.4}$$

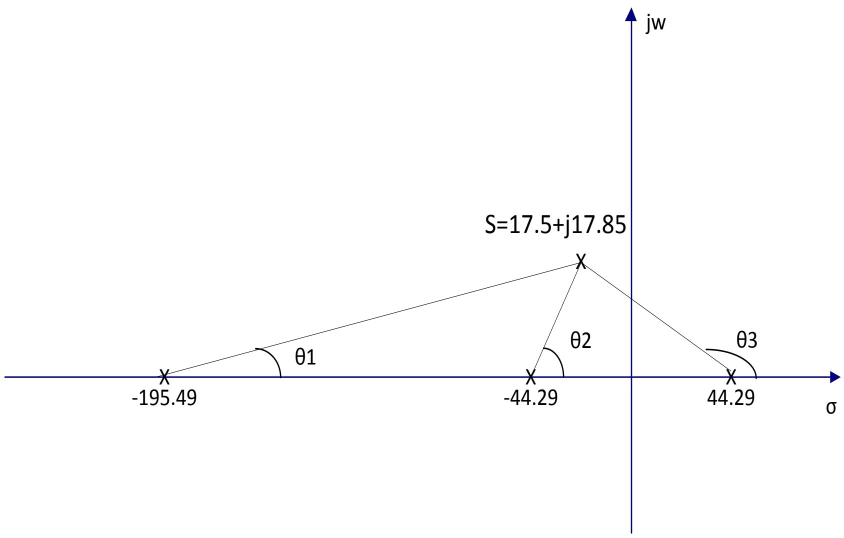

Figure 5. 6. Controller angle determination on the complex plane

Angle of the poles is determined taking arctan of the ratio dominant pole imaginary part to distance of the pole to the dominant pole real part.

First pole angle is

$$\theta_{p1} = \arctan\left(\frac{17.85}{195.49-17.5}\right) = 5.7279° \tag{5.5}$$

Second pole angle is found as:

$$\theta_{p1} = \arctan\left(\frac{17.85}{44.29+17.5}\right) = 33.6761° \tag{5.6}$$

Third pole angle is determined as:

$$\theta_{p3} = 180 - \arctan\left(\frac{17.85}{44.29+17.5}\right) = 163.8850° \tag{5.7}$$

Using relation

$$\theta_c - 5.7279 - 33.6761 - 163.885 = -180° \quad (5.8)$$

Controller angle is found as:

$$\theta_c = 23.289° \quad (5.9)$$

This angle indicates the location of the adding zero as seen in Figure 5.7. The zero of the controller is far from the real part of the dominant poles is

$$z1 = \frac{17.85}{\tan(23.289)} = 41.4692 \quad (5.10)$$

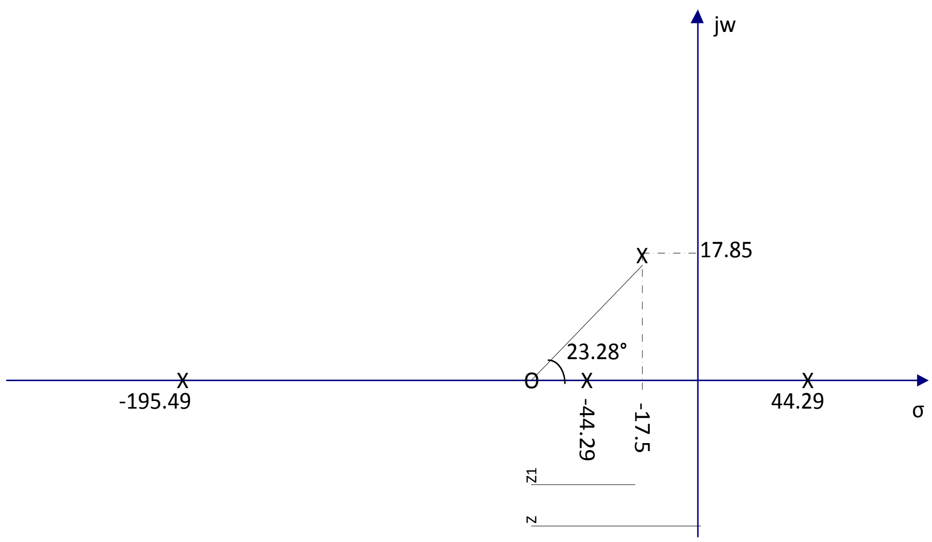

Figure 5. 7. Determining zero location of the controller

The location of the zero is left side of the dominant poles and is specified to adding real part of the dominant pole to z1. The location of the zero is determined as:

$$z = -(41.4692 + 17.5) = -58.9692 \quad (5.11)$$

(5.11) is on the real part of the *s*-plane.

The gain of the controller (K_c) can be found using

$$\left| K_c(s + 58.9692)\frac{20406.6652}{(s+195.5)(s+44.29)(s-44.29)} \right| = 1 \quad (5.12)$$

at $s_d = -17.5 \pm j\,17.85$.

$$K_c = 0.2312 \tag{5.13}$$

and yields,

$$G_c(s) = 0.2312(s + 58.9692) \tag{5.14}$$

PD controller is determined with respect to performance parameters.

Transfer function of the PD controlled system is

$$G_c(s)G(s) = \frac{4718\,s + 278142.77}{s^3 + 195.50\,s^2 + 1962\,s + 383559.3} \tag{5.15}$$

and root locus of the PD controlled system is shown in Figure 5.8. The system is stable with PD compensator as seen in Figure 5.8 and Figure 5.9. Proportional gain (K_p) is 0.2312*58.9692=13.63 and Derivative gain (K_d) is 0.2312 from controller parameters.

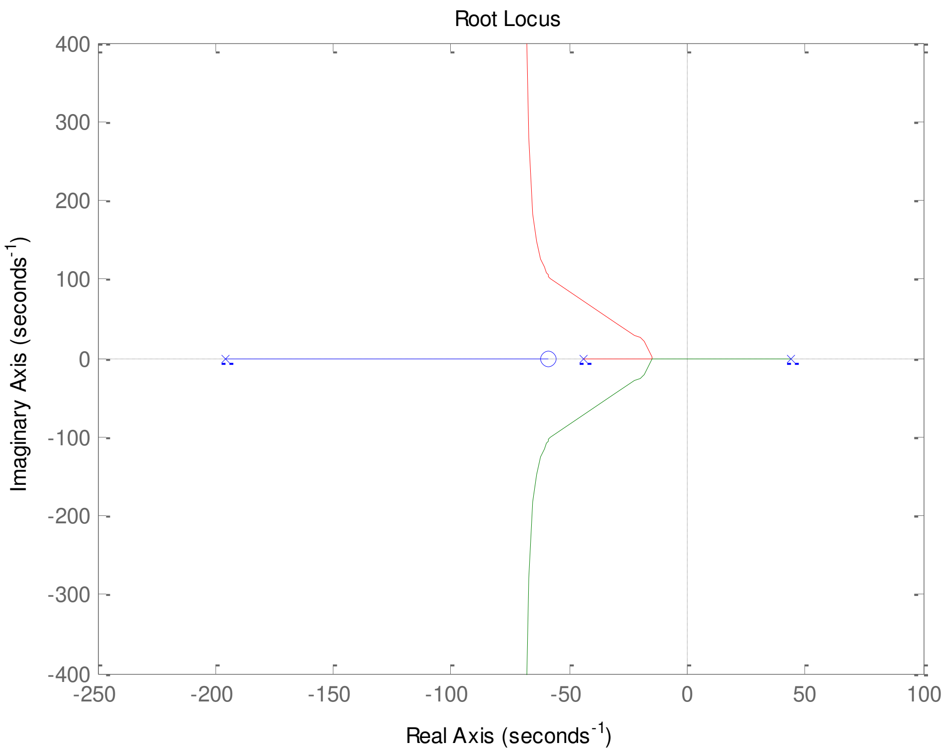

Figure 5. 8. Root locus of the system with PD controller

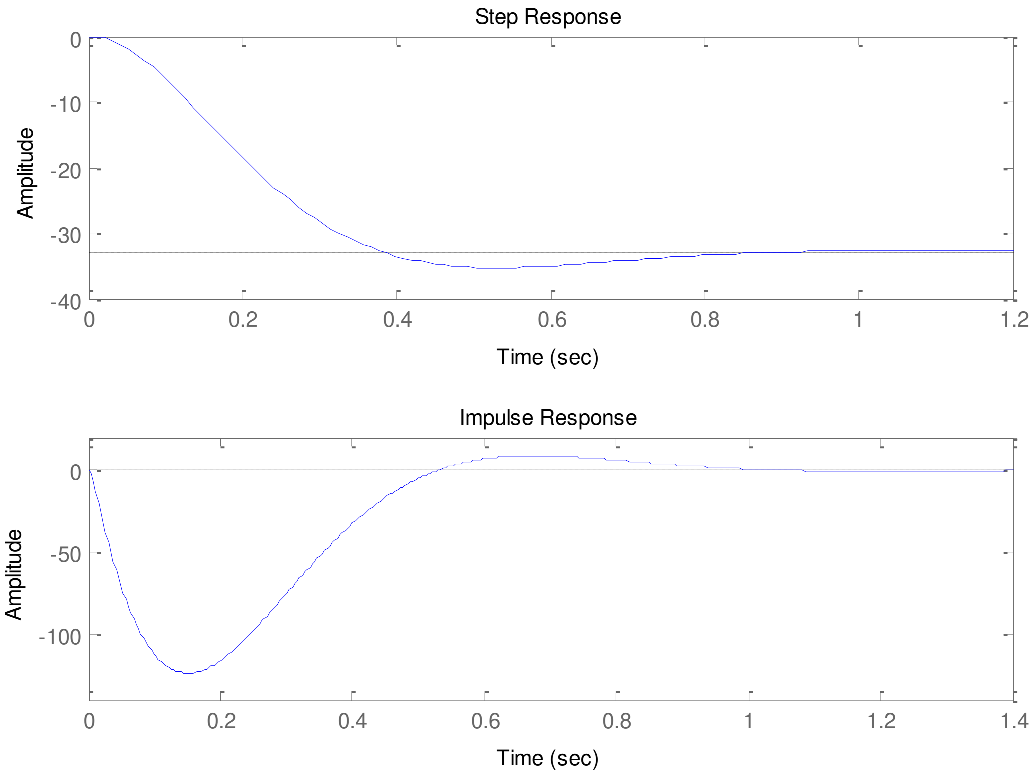

Figure 5. 9. Step and impulse response for PD controller

5.5.2 Phase-Lead Controller Design

Phase-lead controller essentially yields an appreciable improvement in transient response and small change in steady-state accuracy. It may accentuate high-frequency noise effects. This compensator adds a pole and a zero to the transfer function.

Phase-lead controller is defines as:

$$G_c(s) = \frac{K_c(s+z)}{s+p} \tag{5.16}$$

where K_c is the controller gain, z is the zero and p is the pole of the controller.

Phase-lead controller parameters are found using Root Locus Design GUI that is opened for use by Prof. Dr. Hadi Saadat at his personal web page [40]. The GUI work with MATLAB and the overview is seen in Figure 5.10.

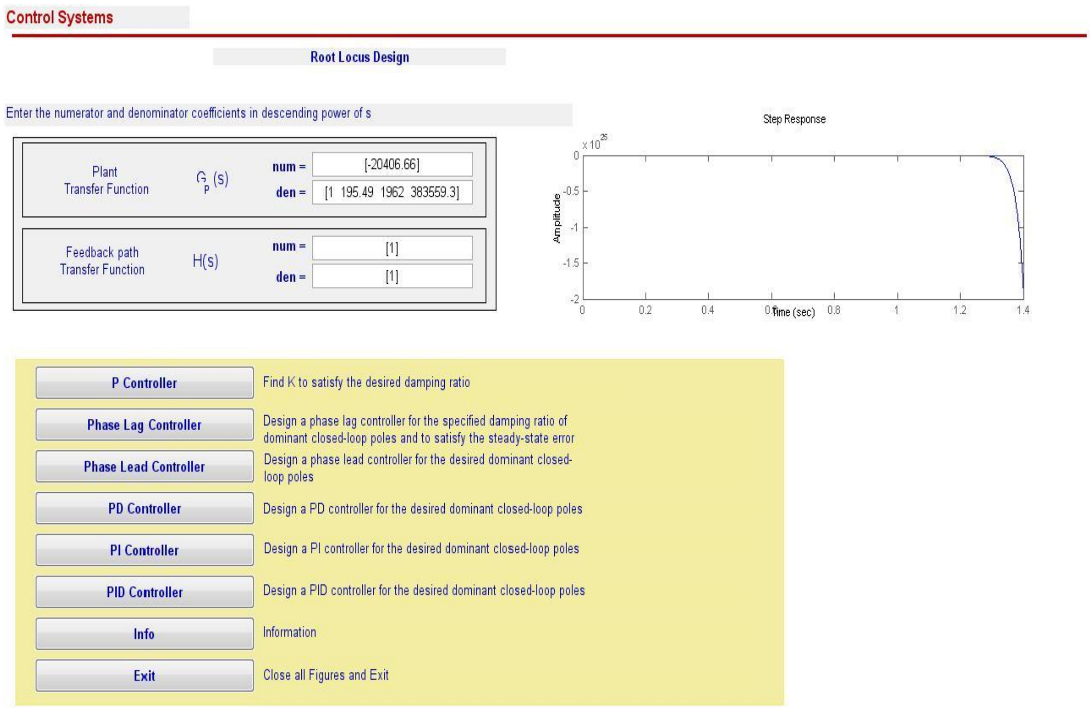

Figure 5. 10. Root locus design GUI

All basic controllers can be designed using this GUI. The transfer function of the system is entered in the GUI and phase-lead controller button is selected. Phase-lead controller design GUI is opened as seen in Figure 5.11.

The domianant comlex poles that is defined as in equation (5.2) are entered to the GUI and DC gain selected. Find G_c (s) button is pressed. The GUI performes the phase-lead compensator algorithm, and finds the phase-lead compensator transfer function and controlled open-loop transfer function as seen in Figure 5.11.

Compensator Transfer function is as follows:

$$G_c(s) = \frac{14.15\,(s+42.32)}{s+33.7} \tag{5.17}$$

Compensated open-loop Transfer function:

$$G_c(s)G(s) = \frac{-288821.6554(\,s+42.32)}{(s+195.5)(s+44.29)(s+33.7)(s-44.29)} \tag{5.18}$$

Is found using phase-lead design GUI.

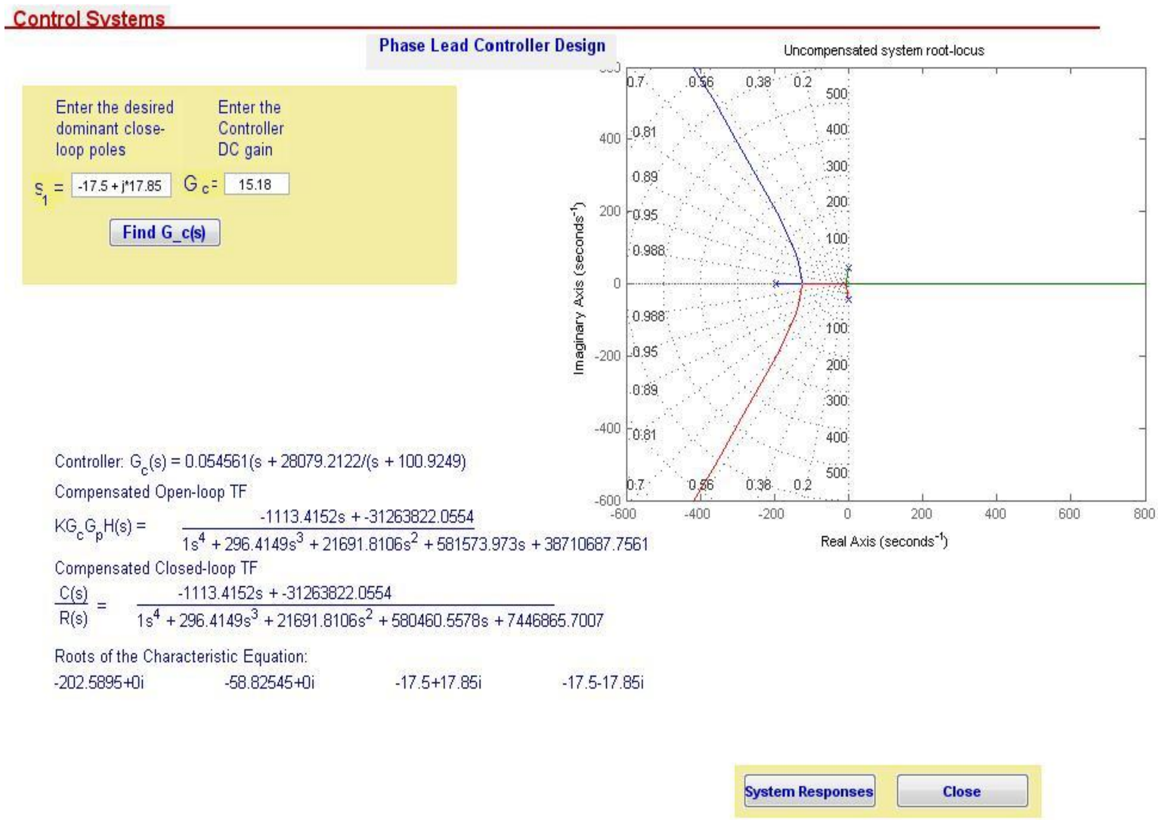

Figure 5. 11. Phase-lead controller design GUI

The compensated system is stable with phase-lead controller is shown on the root locus plot in Figure 5.12. Right half-plane pole is transferred to left-half plane. System works with desired performance parameters for 15.18< K_c <17.77. For best performance controller gain is selected as 15.18.

Step and Impulse Response curve is plotted in Figure 5.13. Step response curve shows that the system response parameters are well at presence of reference variation. Settling time is good for the system. Overshoot is enough small. Impulse response graph shows that the controller suppresses the unexpected disturbance.

Two- different weight is utilized on the SAEMSS with solenoid type as seen in Figure 5.14. The pulse-widths of the system for weights is different. The system with u-type electromagnet is worked and the photo is given in Figure 5.15.

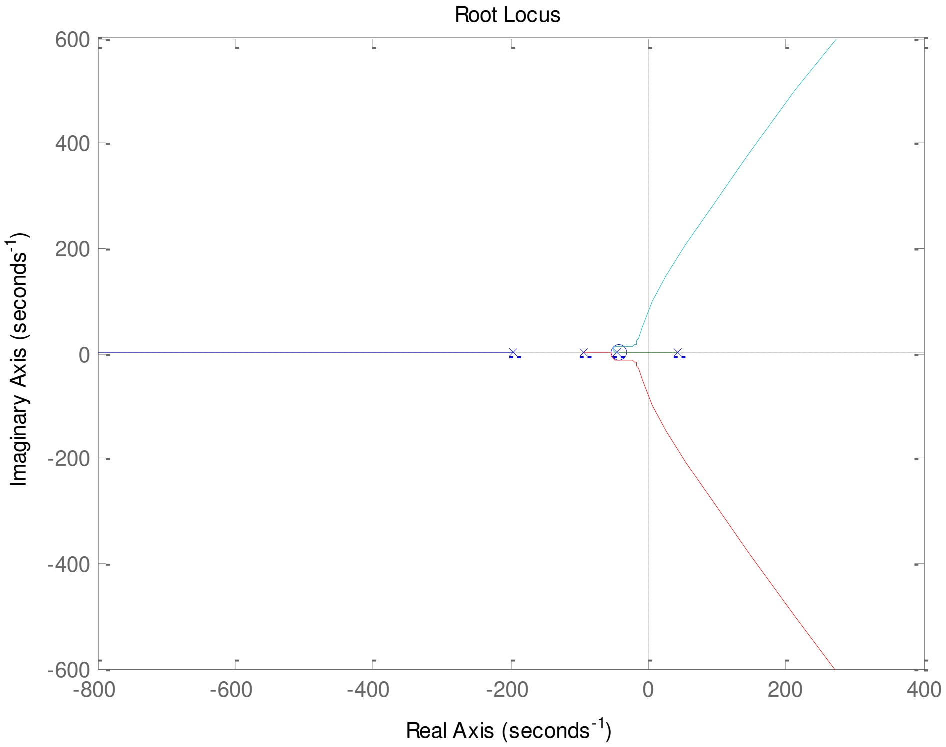

Figure 5. 12. Root locus of the system with phase-lead controller

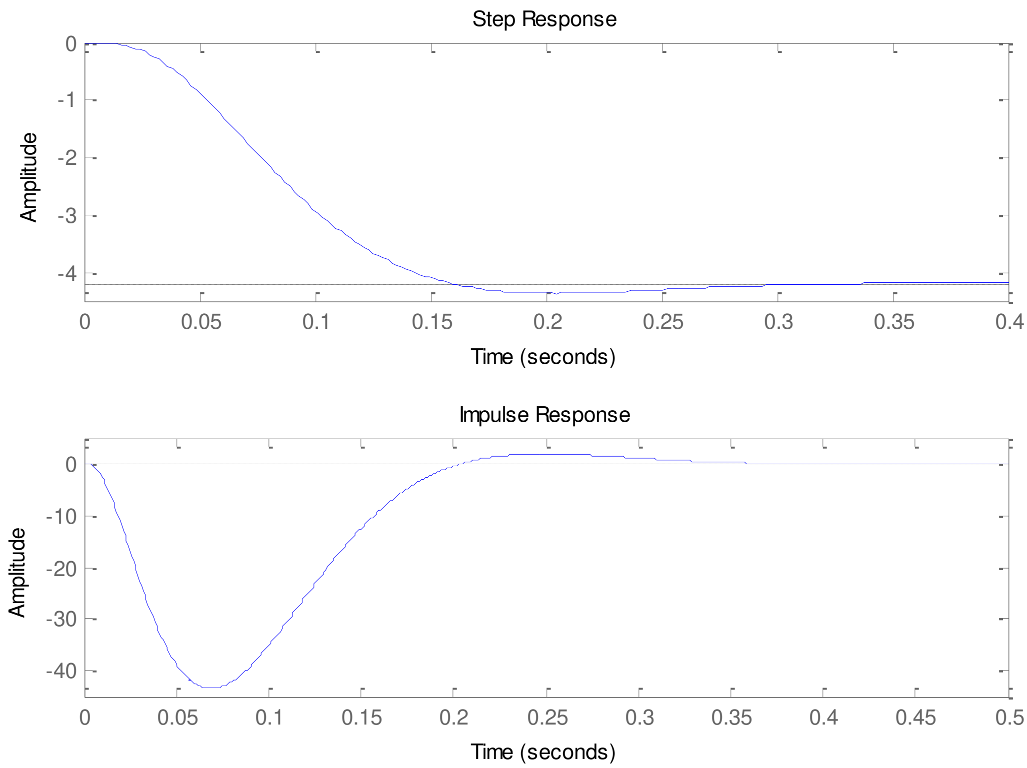

Figure 5. 13. Step and impulse response of phase-lead controlled system

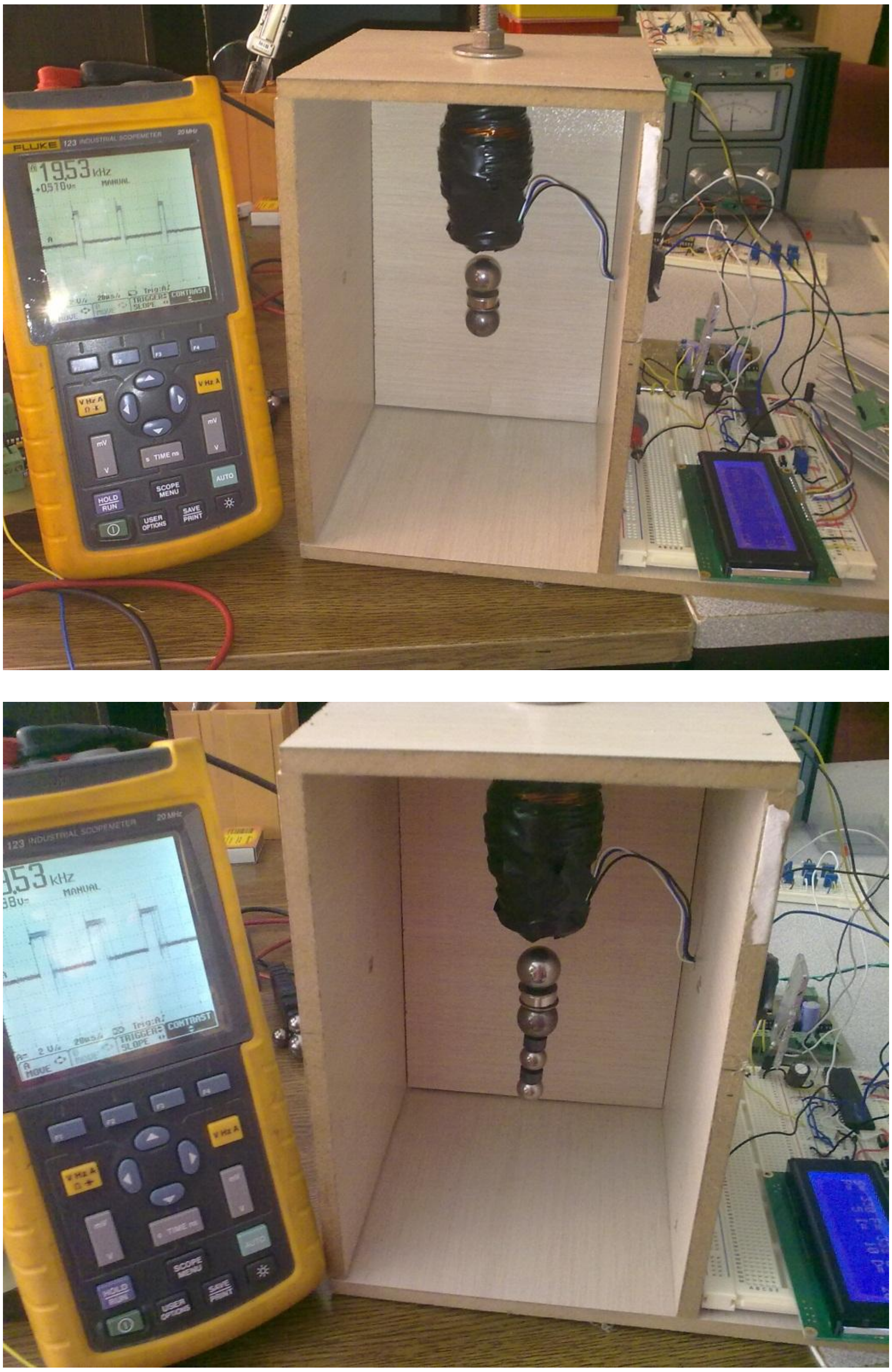

Figure 5. 14. SAEMSS using solenoid type electromagnet with two different weights

Figure 5. 15. SAEMSS using u-type electromagnet

5.6 Summary

The system has a pole on the right-half plane of the s-plane. So, the system is unstable without controller. Root Locus approach is introduced for controller design. The selected controller must carry the right-half plane pole to left side or cancel. So, the controller must add zero to the system. Therefore, two–different (PD and Phase-Lead) controllers are designed. PD controller is designed using PD compensator design technique by hand. Phase-Lead Controller is designed using a Root Locus Design GUI with MATLAB. Root locus of the compensated system is plotted and the effect of the controller can be seen on this plot. Phase-Lead Controller is better than PD controller in terms of trajectory tracking and rejecting disturbance as seen in Figure 5.9 and Figure 5.13. Settling time of the phase-lead controller is about 0.3sec but 1 sec for PD controller.

CHAPTER 6

SOFTWARE FOR SINGLE AXIS MAGNETIC LEVITATION

6.1 Introduction

Software is the soul of the system as hardware is the body. Software is very important to realize desired control algorithms. DSPIC30F4011 is selected as a microcontroller. The features of the DSPIC30F4011 are given in chapter 4. MPLAB IDE (Microchip Product Library Integrated Development Environment) is used as an editor and MPLAB C Compiler is used as a compiler of the program. Generated hex code is loaded to dsPIC using USB PIC Programmer with Us-Burn software. MATLAB is used as a simulator of the system. Parameters of the controllers are calculated using written program in MATLAB and stability and response of the system with controller can be seen using rlocus, step and impulse functions.

6.2 MPLAB IDE

MPLAB Integrated Development Environment (IDE) [41] is a free for use, integrated toolset for the development of embedded applications employing Microchip's PIC® and dsPIC® microcontrollers. MPLAB IDE runs as a 32-bit application on MS Windows®, is easy to use and includes a host of free software components for fast application development and super-charged debugging.

6.3 MPLAB C Compiler

MPLAB C Compiler [42] is the highly optimized compilers for the PIC18 series microcontrollers, high performance PIC24 MCUs, dsPIC digital signal controllers and PIC32MX MCUs. Or, use one of the many products from third party language tools vendors. Most integrate into MPLAB IDE to function transparently from the MPLAB project manager, editor and debugger.

6.4 Developed Algorithm in MPLAB

Flowchart of the developed algorithm is shown in Figure 6.1. The program that is developed and compiled at MPLAB IDE is run on the 30F4011.

At the start of the program, the header files are loaded. Analog to Digital Converter (ADC) output is defined as 10-bit. Various fuses are specified. Used crystal is introduced. The pins that communicate the LCD are defined. LCD run command is activated. CCP unit of the dsPIC is configured for ADC and PWM's output. Timer2 is set for the period of the PWM. Enter the while (1) loop (infinity loop). Analog distance information that is output of the distance sensor is took and converted to digital one using ADC unit with *read_adc* command. If analog to digital conversion is finished, ADC Interrupt flag bit is set high. When ADC INT appears abruptly, program enters the interrupt subroutine. In the subroutine, the error is calculated with respect to reference airgap. The control algorithm is applied using the error signal and output duty is determined for PWM signal. Output signal is used for driving the MOSFET for controlling the electromagnet to levitate the system. Updated information (Controller gains, sent PWM duty, measured distance) is sent to LCD then exit the interrupt routine. The program returns the while (1) loop. The program waits until an interrupt occurring to do the same procedure for levitating the system.

6.5 Us-Burn PIC/dsPIC Programmer

Us- Burn (see in Figure 6.2) [43] is a programmer for Microchip PIC10F/12F/16F/18F/24F and dsPIC30F/33 family using Brenner-8 via USB. PIC series is programmed with Brenner socket but for programming dsPIC is needed extra socket that is connected output pins of the Brenner-8. Firstly, select the PIC family and socket type of the pic then press the identify button in the opened page of the program. If PIC is not broken the Program recognizes the attached PIC. Then the created hex file using MPLAB C Compiler is selected and loaded to dsPIC select HEX-file as a source and write HEX-File into PIC buttons.

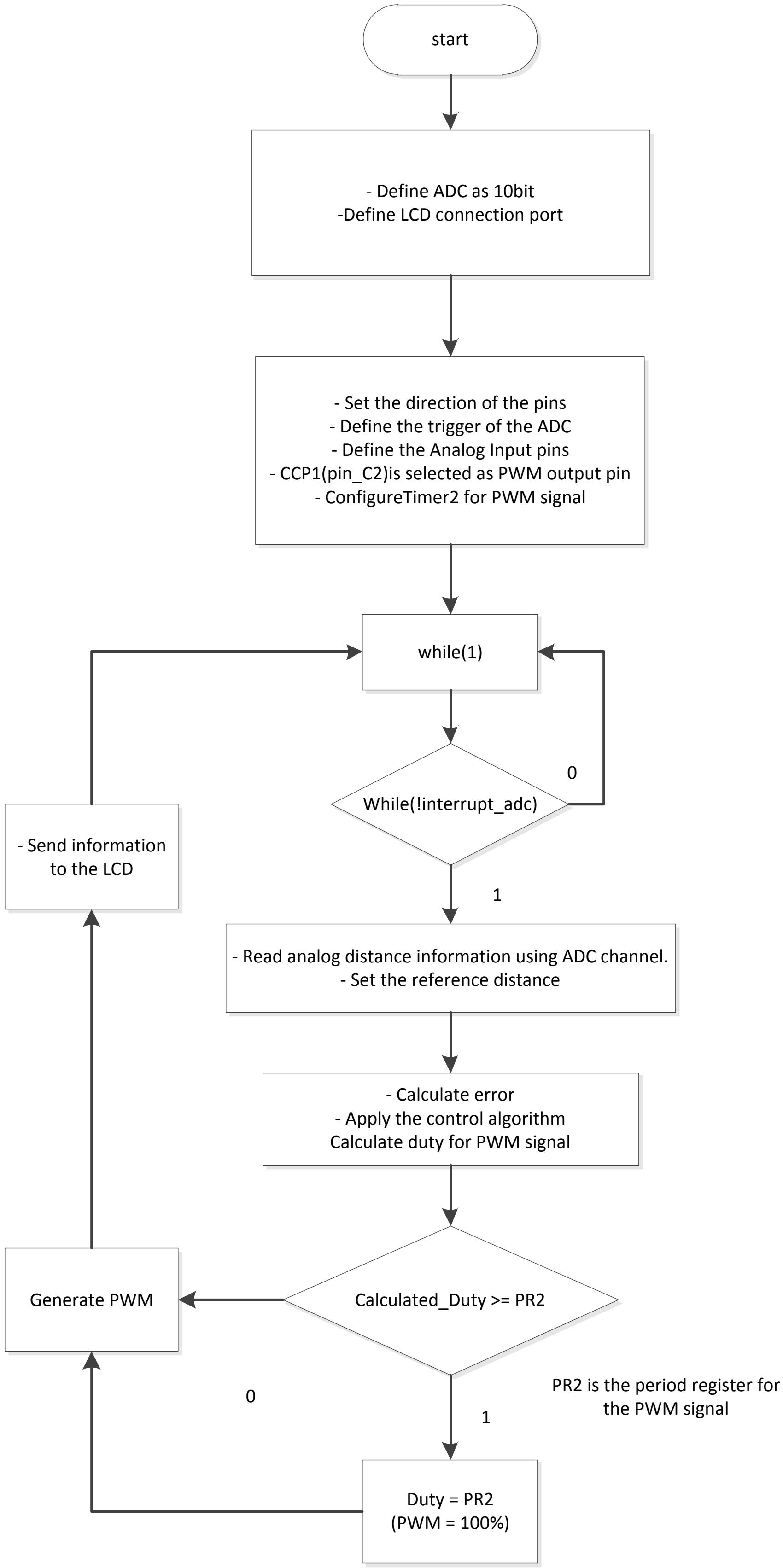

Figure 6. 1. Flowchart of the developed algorithm for magnetic levitation

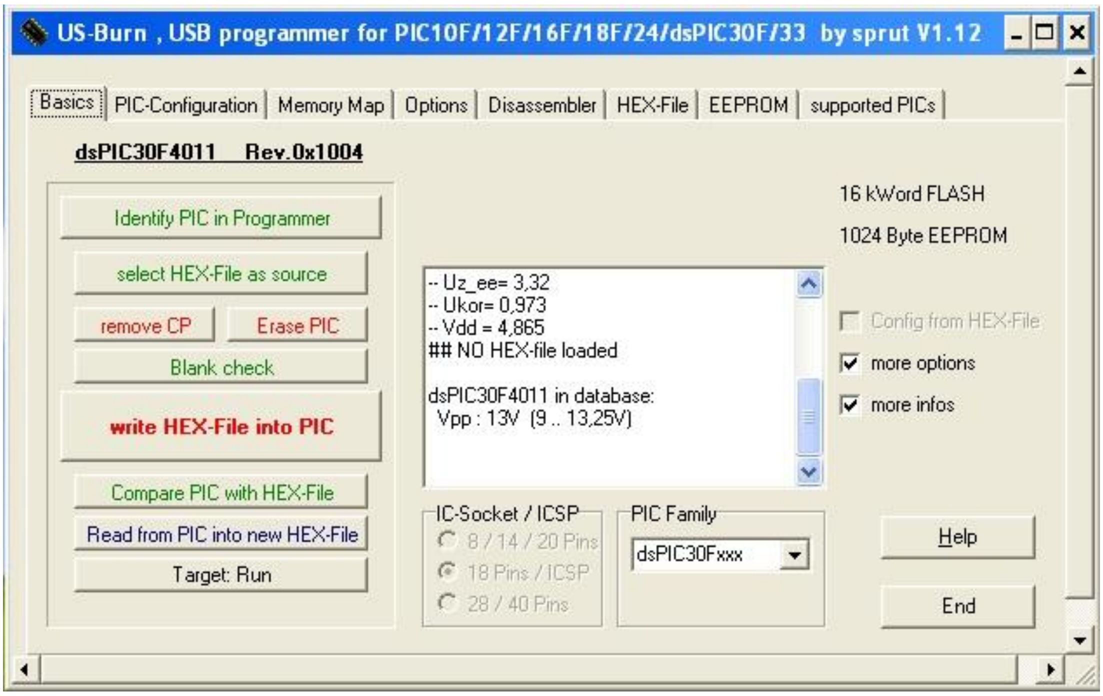

Figure 6. 2. US-Burn PIC programmer overview

6.6 MATLAB

Matrix Laboratory (MATLAB) is a programming environment for algorithm development, data analysis, visualization, and numerical computation. Using MATLAB, you can solve technical computing problems faster than with traditional programming languages, such as C, C++, and FORTRAN [39].

Although MATLAB is intended primarily for numerical computing, an optional toolbox uses the MuPAD symbolic engine, allowing access to symbolic computing capabilities. An additional package, Simulink, adds graphical multi-domain simulation and Model-Based Design for dynamic and embedded systems [39].

In 2004, MATLAB had around one million users across industry and academia. MATLAB users come from various backgrounds of engineering, science, and economics. MATLAB is widely used in academic and research institutions as well as industrial enterprises [39].

Stability and response of the system is analyzed using written program in MATLAB. Firstly system parameters are entered to the program and determined the transfer function of the system. Dominant complex poles are defined. Controller parameters are found with respect to dominant poles. Finally, system stability is seen using root locus and system response is simulated using step and impulse functions with designed controller.

The program written in MATLAB for controller is given following.

```
%sembolik olarak transfer fonksiyon ve state space representation
clear all
clc

syms m g R L1 C I0 x0 b s Kp Kd Ki
C=(m*g*x0^2)/(I0^2)
Kz1=((2*b*C*I0)/(m*L1*x0^2));
Kp1=R/L1;
Kp2=(-2*C*(I0^2))/(m*x0^3);

%transfer function in symbolic
p3=1;
p2=Kp1;
p1=Kp2;
p0=Kp1*Kp2;
num=[Kz1];
den=[p3 p2, p1, p0];
pretty(num)
pretty(den)

%state state representation in symbolic
A11=-Kp1;
A31=(-2*C*I0)/(m*x0^2);
A32=(2*C*I0^2)/(m*x0^3);
A=[A11 0 0; 0 0 1 ;A31 A32 0]
B=[1/L1; 0; 0]

%transfer function elede edilmesi
g=9.81; %m/s^2
%m=input('please enter the MASS in KG of the levitated object : ');
%x0=input('please enter the REFERENCE DISTANCE in meters : ');
%I0=input('please enter the CURRENT in AMPER on the reference point
: ');
%R=input('please enter the RESISTANCE of the coil : ');
%L1=input('please enter the IDUCTANCE of the coil in Henry : ');
%b=input('please enter the Sensor GAIN : ');
m=7.5; %mass
I0=11.87;% reference current
x0=0.01; %referance
R=3.87; %resistance
L1=0.019796; %inductance
b=244.4; %sensor gain

C=(m*g*x0^2)/(I0^2)
Kz1=((2*b*C*I0)/(m*L1*x0^2))
Kp1=R/L1
Kp2=(-2*C*(I0^2))/(m*x0^3)

%transfer function numerically
p3=1;
p2=Kp1;
```

```
p1=Kp2;
p0=Kp1*Kp2;
num=[Kz1]
den=[p3 p2, p1, p0]
GH=tf(num,den)
pole(GH)
zero(GH)
rlocus(GH);
figure, step(GH)

%state space numerically
A11=-Kp1;
A31=(-2*C*I0)/(m*x0^2);
A32=(2*C*I0^2)/(m*x0^3);
A=[A11 0 0; 0 0 1 ;A31 A32 0]
B=[1/L1; 0; 0]
C1=[0 b 0]
D=0
sys = ss(A,B,C1,D);
sys_tf=tf(sys)
rlocus(sys_tf)

i=sqrt(-1);
dr=input('please enter the damping ratio : ')
if(0<dr<1)
else
    while((0>dr & dr>1))
        dr=input('please enter the damping ratio 0< dr <1 : ')
    end
end
nf=input('please enter the natural frequency : ')
s1=-dr*nf+i*nf*sqrt(1-dr^2)
s2=-dr*nf-i*nf*sqrt(1-dr^2)
P=pole(GH);
[m,n]=size(P);
for k=1:m
if P(k)<0
    q(k)=radtodeg(atan((imag(s1))/abs(P(k)-real(s1))))
end
if P(k)>0
    q(k)=180-radtodeg(atan(imag(s1)/(P(k)-real(s1))))
end
end
qc=q(1)+q(2)+q(3)-180

s=17.5+i*17.85

KPD=abs((s+58.9692)*(num/((s+P(1))*(s+P(2))*(s+P(3)))));

%PD Controller
KcPD=1/KPD
GPD=KcPD*tf([1 58.9692],[1])
TPD=GPD*GH
figure, rlocus(TPD)

%phase lead controller
KcPL=46.9;
GPL=KcPL*tf([1 41.5],[1 92.694])
TPL=GPL*GH
figure, rlocus(TPL)
```

6.7 Summary

Digital systems is very effective than analog systems because of easy modification. Control of the system is applied using digital controllers. Software is very important to realize desired digital control algorithms. To operate system some program are used to write program and to load the written program in to MCU. Developed algorithm for control of the system is utilized successfully. The algorithm is written in .MATLAB is used for simulating system with desired controllers. Performance of the system response is analyzed using rootlocus, step and impulse functions.

CHAPTER 7

CONCLUSION

EMS systems are nonlinear and open loop unstable. Firstly, the nonlinear controller is linearized using Taylor series expansion method at equilibrium position. Using obtained linearized equation transfer function is derived. PD controller is designed to stable the system by compensation method by hand with defined performance factors. Phase-lead controller is optimized using Root Locus Design GUI written by Prof. Saadat. Controller gains are found using mentioned methods in chapter 5.5. System is successfully controlled experimentally by using dsPIC30F4011 MCU for both methods.

Different weights in the range of 150 gr with neodium magnet are levitated using solenoid type electromagnet. 7.5 kg iron bar levitated using u-type electromagnet.

PD and phase-lead controllers are applied to these single-axis EMS. Phase-lead controller out performs the PD controller. In terms of disturbance and trajectory tracking, phase-lead is very better than PD. Settling time of the phase-lead controller is very less than PD and approximately 0.25sec. Overshoot is small in both methods.

Digital controllers are more flexible than analog controllers. While using digital controllers, there is no need to change hardware design. Algorithms those are written for MCU has simple form and easy to apply experimentally. 10 bit analog input and 16-bit PWM output is utilized using MCU.

In this work, Hall-effect sensor is used to measure in solenoid type single-axis EMS. Inductive sensor is used to detect position of the levitated object in u-type EMS.

For future studies can be done using more effective control techniques such as fuzzy, H^{∞}, adaptive, sliding mode control methods. Besides that EMS system can be constructed as half (2-axis) and full body (4-axis) types. Using laser sensor for the measurement of the airgap would be a good choice if sufficient budget obtained. DSP would be utilized instead of MCU because of high speed processing, excellent computation accuracy, 12-bit analog input and 16-bit PWM output, 32-bit fixed or floating point operation.

REFERENCES

[1] H.W. Lee, H.C. Kim and J. Lee (2006). Review of Maglev Train Technologies, *IEEE Transactions on Magnetics*, **42(7)**, 1917-1925.

[2] B. V. Jayawant. (1981). Electromagnetic suspension and levitation, *Rep.Prog. Phys,* **44**, 411-477.

[3] T. H. Wong. (1986). Design of a Magnetic Levitation Control System-An Undergraduate Project, *IEEE Transactions on Education*, **E-29(4)**, 196-200.

[4] M. Morishita, T. Azukizawa, S. Kanda, N. Tamura and T. Yokoyama. (1989). A New Maglev System for Magnetically Levitated Carrier System, *IEEE Transactions on Vehicular Technology*, **38(4)**, 230-236.

[5] D. Cho, Y. Kato and D. Spilman. (1993). Sliding Mode and Classical Control of Magnetic Levitation System, *IEEE Control Systems*, **13(1)**, 42-48.

[6] W. Barie and J. Chaiasson. (1996). Linear and nonlinear state-space controllers for magnetic levitation, *International Journal of Systems and Science*, **27(11)**, 1153-1163.

[7] W. G. Hurley, Senior Member, IEEE, and W. H. Wölfle. (1997). Electromagnetic Design of a Magnetic Suspension System, *IEEE Transactions on Education*, **40(2)**, 124-130.

[8] Y.S. Shiao. (2001). Design and Implementation of a Controller for a Magnetic Levitation System, *Proc. Natl. Sci. Counc. ROC(D),* **11(2)**, 88-94.

[9] A. Hajjaji and M. Ouladsine. (2001). Modeling and Nonlinear Control of Magnetic Levitation Systems, *IEEE Transactions on Industrial Electronics*, **48(4)**, 831-838.

[10] J. C. Shen. (2002). H∞ Control and Sliding Mode Control of Magnetic Levitation System, *Asian Journal of Control*, **4(3)**, 333-340.

[11] Z. J. Yang, K. Miyazaki, C. Z. Jin and K. Wada. (2002). Physical Parameter Identification of a Magnetic Levitation System under a Robust Nonlinear Controller, *15th Triennial World Congress*, Barcelona, Spain.

[12] R. R. Gomes, Student Member, IEEE, D. C. B. V. Silva, Student, and J. L. S. Neto, Supervisor, Member, IEEE. (2003). Electromagnetic Levitation Using MATLAB Real Time Control Toolbox, *International Symposium on Industrial Electronics*, **2**, 1144-1146.

[13] P.S. Shiakolas, Member, IEEE, S. R. Schenck, D. Piyabongkarn and I. Frangeskou. (2004). Magnetic Levitation Hardware-in-the-Loop and MATLAB-Based Experiments for Reinforcement of Neural Network Control Concepts, *IEEE Transactions on Education*, **47(1),** 33-41.

[14] H. Huajie and L. Jie. (2004). The Influence of Filter on Stability of Electromagnetic Levitation System, 8th *International Conference on Control, Automation, Robotics and Vision*, Kunming, China, **2**, 1379-1383.

[15] K. A. Lilienkamp and K.Lundberg. (2004). Low-cost magnetic levitation project kits for teaching feedback system design, *American Control Conference*, **2**, 1308-1313.

[16] S. Banerjee, D. Prasad and J. Pal. (2006). Design, implementation, and testing of a single axis levitation system for the suspension of a platform, *ISA Transactions*, **46(2)**, 239-246.

[17] Z. Yang and G. Pedersen. (2006). Automatic Tuning of PID Controller for a 1-D Levitation System Using a Genetic Algorithm - A Real Case Study, *International symposium on Intelligent Control*, Munich, Germany, 3098-3103.

[18] F. Gürleyen and Ç. Bahadır (2006). Manyetik Askı Sistemleri için Dayanıklı PID ve Değişken Yapılı Kontrol, *ELECO'06*, Bursa, Türkiye.

[19] S. Öztürk, S. Kizir, Z. Bingül and C. Oysu. (2007). Manyetik Süspansiyon Sisteminin Gerçeklenmesi ve Kontrolü, *TOK'07 Bildiriler Kitabı*, İstanbul, Türkiye, 95-100.

[20] J. Tang. (2007). Magnetic Levitation Systems Using Analog and Digital Phase-Lead Controllers, *American Society for Engineering Education Conference*, Hawaii, America, 345-354.

[21] Q. H. Guo, D. S. Li, Z. Y. Lu, W. Wang and L. Z. Ye. (2008). Research on a Maglev Ball Control System Based on DSP2812, *23rd Progress in Electromagnetics Research Symposium,* Hangzhou, China, 536-539.

[22] M. Deshpande and B. L. Mathur. (2009). A Novel Displacement Sensor for Magnetic Levitation, *International Journal of Recent Trends in Engineering*, **1(3)**, 21-24.

[23] L. Wang, Jin-Liu(2009). Sliding Mode Control of CNC Electromagnetic Levitation System Based on Feedback Linearization, *Chinese Control and Decision Conference (CCDC'09)*, Chinese, 2706-2709.

[24] I. Ahmad and M. A. Javaid. (2010). Nonlinear Model & Controller Design for Magnetic Levitation System, *International conference on Signal Processing, Robotics and Automation (ISPRA '10),* Cambridge, UK, 324-328.

[25] S. A. Green, R. S. Hirsch, and K. C. Craig. (1995) Magnetic levitation devices teaching aid for mechatronics at Rensselaer, *in Proc. ASME IMECE Dynamic Syst. Control Div*.

[26] K. Craig, T. Kurfess, and M. Nagurka. (1998).Magnetic levitation tested for controls education*, in Proc. ASME, Dynamic Syst. Control Div.*, **DSC-64**, 83–88.

[27] Honeywell Inc. Hall Effect Sensing and Application USA. Available via URL http://www.emt.jku.at/education/Inhalte/pr_emtsens/unterlagen_downloads/hallbook.pdf

[28] UGN3503 datasheet, Continuous-Time Ratiometric Linear Hall Effect Sensor ICs Allegro, Available via URL, www.allegromicro.com/en/Products/Magnetic-Linear-And-Angular-Position-Sensor-ICs/Linear-Position-Sensor-ICs/A1301-2.aspx

[29] Inductive Proximity sensors, Alter Copp. Available via URL: http://www.altechcorp.com/HTML/Sensors_Standard-A.html

[30] XSA-P30AB110, Inductive Proximity Sensor, Telemecanique, Available via URL: http://www.neweysonline.co.uk/neweys/pdf/Telemecanique_Inductive_Proximity_Sensors_Osiprox_Technical.pdf

[31] dsPIC30F4011, datasheet. Microchips, Available via URL: http://www.microchip.com/wwwproducts/Devices.aspx?dDocName=en010337

[32] 6N137 datasheet, Toshiba, Available via URL: http://www.semicon.toshiba.co.jp/eng/product_detail/opto/coupler/1260156_13597.html

[33] BC237, npn transistor, Fairchild Available via URL: http://www.datasheetcatalog.org/datasheet/fairchild/BC237.pdf

[34] MIC4422, 9A-Peak Low-Side MOSFET Driver, Micrel, Available via URL: http://www.micrel.com/_PDF/mic4421.pdf

[35] C.W. Lander. (1993). Power Electronics. Third Edition. ISBN: 0-07-707714-8, *Typeset by Thomsan Press (India) Ltd. New Delhi. Printed in Singapore*.

[36] IXTQ170N10P, Power Mosfet, IXYS, Available via URL: http://ixapps.ixys.com/DataSheet/DS99176F(IXTT-TQ-TK170N10P).pdf

[37] J. Hogerman. (1995), Calculating Optimal Snubbers, *Hogerman Technology*

[38] K. Ogata, (1990) Modern control Engineering, Second Edition, Prentice- *Hall International Editions*, ISBN: 0-13-598731-8

[39] MATLAB R2011a, Available via URL: http://www.mathworks.com/products/matlab/

[40] H. Saadat, Root Locus Design Gui, http://www.saadat.us/matlabgui.htm

[41] MPLAB Integrated Development Environment, Available via URL: http://www.microchip.com/stellent/idcplg?IdcService=SS_GET_PAGE&nodeId=1406&dDocName=en019469&redirects=ide

[42] MPLAB C Compiler, Available via URL: http://www.microchip.com/stellent/idcplg?IdcService=SS_GET_PAGE&nodeId=1406&dDocName=en010065

[43] Us-Burn, Available via URL: http://www.microchip.com/stellent/idcplg?IdcService=SS_GET_PAGE&nodeId=1406&dDocName=en010065